Naval Research Laboratory
Washington, DC 20375-5320

NRL/MR/6650--93-7357

Theory and Modeling of Thermal Reaction Propagation in Beam-Initiated Explosives

J. B. Aviles, Jr.

Consultant, SFA, Inc.

A. Stolovy

Directed Energy Effects Branch
Condensed Matter and Radiation Sciences Division

June 10, 1993

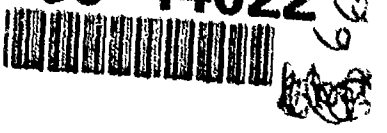

Approved for public release, distribution is unlimited.

REPORT DOCUMENTATION PAGE

Form Approved OMB No. 0704-0188

1. AGENCY USE ONLY (*Leave Blank*)	2. REPORT DATE	3. REPORT TYPE AND DATES COVERED
	June 10, 1993	Final Report

4. TITLE AND SUBTITLE

Theory and Modeling of Thermal Reaction Propagation in Beam-Initiated Explosives

5. FUNDING NUMBERS

PE - 61153N-12
TA - RR012-02-44
WU - 66-2821-0-3

6. AUTHOR(S)

J.B. Aviles Jr.* and A. Stolovy

7. PERFORMING ORGANIZATION NAME(S) AND ADDRESS(ES)

Naval Research Laboratory
Washington, DC 20375-5320

8. PERFORMING ORGANIZATION REPORT NUMBER

NRL/MR/6650--93-7357

9. SPONSORING/MONITORING AGENCY NAME(S) AND ADDRESS(ES)

10. SPONSORING/MONITORING AGENCY REPORT NUMBER

11. SUPPLEMENTARY NOTES

*Consultant, SFA, Inc.

12a. DISTRIBUTION/AVAILABILITY STATEMENT

Approved for public release; distribution unlimited.

12b. DISTRIBUTION CODE

13. ABSTRACT (*Maximum 200 words*)

Previous work on the thermal initiation of energetic materials by particle beams concentrated on uniformly irradiated confined samples. The present report extends the work to situations where only a portion of the material has been irradiated. In some materials (e.g., TATB) only the irradiated region undergoes thermal initiation; in other materials a thermal initiation front has been observed (by thermocouple response) to propagate away from the irradiated region. The frontal speeds are of the order of centimeters per second to tens of centimeters per second. These slow speeds eliminate the possibility of pressure propagation or a deflagration to detonation transition (DDT).

Modeling is based on the interference that at the thermal initiation temperature the material develops a greatly enhance thermal and gaseous diffusivity. This allows the exothermic energy released to propagate into the cold region and forestalls any explosive temperature rise. At a well defined positive R* (the explosion radius) thermal initiation propagation ceases and an explosive temperature rise takes place.

14. SUBJECT TERMS

15. NUMBER OF PAGES

63

16. PRICE CODE

17. SECURITY CLASSIFICATION OF REPORT	18. SECURITY CLASSIFICATION OF THIS PAGE	19. SECURITY CLASSIFICATION OF ABSTRACT	20. LIMITATION OF ABSTRACT
UNCLASSIFIED	UNCLASSIFIED	UNCLASSIFIED	UL

CONTENTS

THEORY AND MODELING OF THERMAL REACTION PROPAGATION IN BEAM-INITIATED EXPLOSIVES

Introduction and Summary

Over the past years the thermal initiation properties of energetic materials have been studied by Stolovy, Namenson, Kidd, Jones, and Aviles [Ref. 1]. These studies have overwhelmingly concentrated on the behavior of small confined samples uniformly irradiated by particles beams. Since thermal losses are greatly reduced, the thermal behavior is essentially adiabatic. The resultant thermal initiation threshold energies and temperatures are important intrinsic properties of the material. In particular there is direct applicability to charged and neutral particle beam weapons lethality in scenarios where energetic materials are irradiated in depth.

This report is concerned with effects that occur after initiation in a situation where only a portion of the material has been irradiated. Given the rapidity with which the temperature rises after initiation in the adiabatic case and given the small thermal conductivity of energetic materials, it would be natural to predict that thermal initiation will occur only in the beam irradiated region that has reached the thermal initiation threshold. However, for certain energetic material, Stolovy, et al have observed thermal initiation fronts propagating away from the beam region. The frontal speeds of various materials are of the order of centimeters per second to tens of centimeters per second. The relatively low speeds eliminate the possibility of pressure waves and the light confinement is not conducive to a deflagration to detonation transition (DDT). Thus some kind of thermal reaction propagation mechanism is indicated. The measured thermal diffusivities at subinitiation temperatures are too low by orders of magnitude to account for these speeds. It is necessary to postulate that a radical transition in transport properties occurs at the thermal initiation temperature. Model equations have been developed for this situation and have been solved analytically (in an appropriate approximation) for the cylindrically symmetric case which obtains in the electron beam experiments. In particular, the time for the initiation front to propagate from the edge of the particle beam of radius a to the radial position R is given by

$$\Delta t = t_q\left[\sqrt{1-(R/R^*)^2} + \ln\left(1-\sqrt{1-(R/R^*)^2}\right)\right]_a^R \qquad (0.1)$$

where

$$R^* = \sqrt{2D_T t_s} \qquad (0.2)$$

The parameters t_q is the time for the temperature in the cold high explosive (HE) to rise to the initiation temperature as a result of propagation. The parameter t_s is the adiabatic time to explosion, i.e., the time after initiation for the HE to reach a very high temperature when there is no outflow of heat. The parameter D_T is an effective thermal diffusivity which pertains only to region of the HE which is above the thermal initiation temperature.

Manuscript approved May 21, 1993.

The most important feature of Eq. (1) is that for values of $R > R^*$ the expression takes on complex values. The theoretical analysis shows that when the front reaches R^* the initiated region $R < R^*$ undergoes a sudden rapid rise in temperature, i.e., an explosion develops. Hence, R^* will be called the explosion radius for the material. If the beam radius exceeds the explosion radius no propagation occurs; the irradiates region then undergoes an adiabatic thermal explosion.

The experimental data for the validation of Eqs. (0.1) and (0.2) are sparse. The initial experiments, which discovered the phenomenon of thermal initiation propagation in HE, were of an exploratory nature. The results, not previously published, are described in Appendix A.1. Unfortunately, the set of experiments [Ref. 2] which were designed to investigate the phenomenon in greater detail did not have the benefit of the present analysis. The beam radii were generally chosen larger than in the initial experiments and the thermocouples used were not as responsive. As a result propagation was obscured. These later experiments are compatible with the theory presented here but do not contribute to its quantitative validation. The initial experiments on PBX-9404, although sparse in data, are sufficient to give order of magnitude values for the parameters t_i and R^*. An estimate of t_e from thermal decomposition reaction parameters then allows a determination of D_T.

Subsequent experiments, designed to validate the present theory, have not been carried out owing to funding limitations. Rather than allow the phenomenon of thermal initiation propagation to remain obscure and unexplored, a fairly ambitions conceptual and theoretical analysis was undertaken. The general theory and the results for particle beam irradiation, i.e., for cylindrical symmetry, are present here. Laser irradiation of a surface (planar symmetry) also produces thermal initiation propagation and has been analyzed theoretically; however the results are not present here since there is insufficient data to make a quantitative analysis. These experiments are also described in Appendix A.1; they clearly indicate a propagating thermal initiation front.

In Section 1 the experimental observations and certain reasonable conclusions are given. Details are found in Appendix A.1 and Reference 2. In Section 2 a conceptual physical description is presented; it is based on the experimental observations, the model which is developed in later sections, and reasonable speculation. Empirical reaction modeling, based on thermal decomposition experiments, is presented in Section 3 and is applied in Section 4 to thermal initiation of materials uniformly irradiated by particle beams. Appendix A.2 shows that, for the limited temperature range involved in thermal initiation propagation, the reaction model can be greatly simplified with impunity. In Section 5 a simple model is presented in which it is assumed that all of the energy liberated by decomposition in the initiated region of the material is transported immediately to the front and used up there to sustain the

propagation of the front. This model helps fix certain useful ideas in a very simple way.

In Section 6, which is quite lengthy and demanding, the fundamental hydrodynamic-reaction equations are examined. Comparison with experimental observations allows for a systematic reduction of the equations until finally only a thermal diffusion-reaction equation remains. This is the basis of the model equations solved in Section 7 and compared with experimental results in Section 8 for the purpose of estimating model parameter.

The establishment of the thermal diffusion-reaction model, which was done in Section 6 is believed to be necessary since the available experimental data is too sparse to validate the model with sufficient conviction.

The analysis shows that, with sufficiently detailed experimental data, reaction parameters above the initiation threshold can be obtained. This is not generally feasible with adiabatic experiments alone.

1. Experimental Observation

The specific physical situations to be modeled are the reaction propagation experiments of Stolovy, Kidd, and Namenson. Recent experiments are described in the FY 90 report: "Reaction Propagation Studies in Beam-Initiated Confined Explosives"[Ref 2]. Past experiments have been reanalyzed and a summary is given in an appendix to this report.

The experiments were performed on short cylinders of HE (Figure 1) which are confined in an aluminum holder (not shown). The beam, which has been collimated, irradiates only the central region of the HE cylinder. The exit window, by which the beam

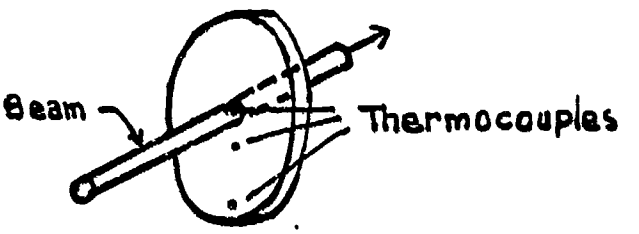

Figure 1

leaves the HE, was designed to be the weakest part of the holder and thus the main part of the structure to be disrupted during an explosion.

The principal objective of the experiments was to determine if the HE was thermally initiated beyond the beam irradiated region and to measure, by thermocouple response, the time of arrival of the initiation front at several radial positions. Four secondary HE were studies: TATB, HBX-1, PBXW-109, PBX-9404.

In the TATB experiments, explosions were weak, with no initiation propagation beyond the beam region. The well known insensitivity of TATB is evidently retained under the conditions of these experiments. In the HBX-1 experiments, the samples exploded with more violence. In the FY 90 set of experiments, no initiation beyond the beam region was observed. In the previous set (see Appendix A.1) in which the beam was narrower and more intense, most (but not all) of the HE was consumed; a propagation velocity of the order of 1 cm/sec was observed. PBXW-109 behavior was generally similar to HBX-1; no quantitative measure of the propagation velocity was obtained.

Initiation propagation is very pronounced in PBX-9404 (94% HMX). In every experiment all of the HE was consumed and a violent explosion occurred. Initiation propagation velocities (See Appendix A.1) in the range 25-50 cm/sec were observed. Laser experiments (Appendix A.1) on confined PBX-9404, in which only one surface of the sample was heated, produced similar results. However, surface temperatures greater than the initiation temperature were

necessary to precipitate propagation.

The general conclusions that have been drawn from the analysis are as follows:

1. Initiation propagation is an intrinsic property of confined HE. The values of the frontal velocities vary widely from one HE material to the other. The observed representative values are: TATB, v = 0; HBX-1, v = 1 cm/sec; PBX-9404, v = 25 cm/sec.

2. In those HE materials in which propagation is present, the explosion is delayed until after significant initiation propagation has occurred. This indicates that heat and probably reactants are transported out of the initiated region into the uninitiated region. Instead of creating an explosion immediately, the energy goes into raising the temperature of the adjacent cold region. This process creates and sustains the front that is observed.

3. Confinement is necessary for thermal initiation in general. However, the strength of the confinement does not appear to have an affect on initiation or propagation. This indicates that the function of confinement is the retention of gaseous reactants. The strength of the confinement affects the violence of the eventual explosion: the higher the pressure at which explosive disruption occurs, the greater the ensuing violence.

4. The evidence is consistent with the concept of an intrinsic limiting propagation radius at which the explosion occurs. In TATB this radius is less than 0.6 cm. In HBX-1 and PBXW-109 the limiting radius is probably less than a centimeter. In PBX-9404 an explosion radius of about 1 cm is indicated.

The relatively slow propagation speeds and weak confinement rule out a DDT or a detonation wave. This is further discussed at the end of the next section.

2. Conceptual Physical Description

The process by which the cylinder of HE proceeds from beam initiation of its central region to eventual explosion can be conceptually broken up into the several phases depicted in Figures 2. a-e. This construct is based in part on experimental observations and in part on the theoretical and modeling analysis presented in Sections 6 and 7.

Figure 2.a. Initially the electron beam heats the cylindrical volume bounded by radius a. The temperature T_1 is less than the initiation temperature T_R. Owing to collimation, the beam will have an approximate top hat profile. Normal thermal diffusion produces a temperature profile with an rms radius given by

$$\langle r^2 \rangle = 2D_o t + a^2 \qquad (2.1)$$

Normal thermal diffusivity of organic HE have $D_o < 10^{-3}$ cm^2/sec. For irradiation time t = 10 sec and collimation radius 0.2 cm, the temperature profile radius will increase by <.04 cm and the flat portion of the profile will decrease by the same order of magnitude. The flat portion of the profile will reach the initiation temperature in an adiabatic manner. In modeling, a top hat profile will be used with an effective radius determined by fitting the model to the experimental data. This effective radius should be somewhat less than the collimation radius.

Figure 2.b. Initiation in the beam region has been achieved. This is a transient phase in which the conditions for propagation are developing. Necessary conditions are:

a) greatly increased thermal diffusivity
b) creation of sufficient heat and mobile reactants to precipitate frontal motion.

The temperature rise tends to be adiabatic before propagation begins. The time duration of this phase is too short for thermocouple measurements. In PBX-9404, it lasts for less than a millisecond . If propagation does not develop, a thermal explosion will develop on this time scale.

Figure 2.c. Propagation begins. Heat and mobile reactants diffuse from the beam region to the front. Cold material is heated up to the initiation temperature T_R. Below T_R, normal diffusion is completely negligible on a millisecond time scale. Above T_R diffusion is very pronounced. The temperature in the central region levels off as a result of the greatly enhanced diffusion and the consequent outflow of heat.

Figure 2.d. A quasi-steady state (QSS) propagation has been achieved. the

temperature profile takes on a Quasi-equilibrium form. Almost all of the energy generated in the initiated region flows to the frontal boundary. The temperature profile continually adjusts itself to the motion of the front. This quasi-equilibrium status is a consequence of the high thermal diffusivity that develops for $T > T_R$.

The greatly enhanced thermal conductivity for $T > T_R$ could be accounted for by the following hypothesis: Once the initiation temperature T_R is reached a profuse generation of mobile reactants develops. The increased mobility accounts for the greater thermal conductivity. The mobility of the reactants (or their diffusion) is curtailed in the cold region beyond the front. Physical changes in the initiated region, e.g., increased porosity, melting, or a solid state phase change, would also contribute to the increased diffusivity in this region. Although there are no direct experimental observations to confirm the above hypothesis, such considerations are very helpful in formulating a model which can account for the observed frontal motion.

Figure 2.e. The initiation front does not propagate indefinitely. As the front recedes from the center region it takes an increasingly longer time for heat generated in the center to be transported to the front. In addition, the quasi-equilibrium temperature at the center is increasing as a result of adjustment to the frontal motion. At a time t^*, a well-defined frontal position R^* is reached for which it is impossible to maintain a quasi-equilibrium situation. At this point in time the temperature in the central region rises above its equilibrium value and, owing to the autoaccelerating nature of the reaction rate, undergoes an explosive rise. The pressure also rises explosively. The weak confinement experiments under analysis are thus abruptly terminated when the pressure exceeds the strength of the confinement; details can't be measured by thermocouple response.

Additional considerations are necessary in the situation (see Figure 3) where one face of a confined HE is in contact with an inert material (usually a metal) which is at a temperature greater than the initiation temperature T_R of the HE. The HE is initially at temperature $T_o < T_R$. Experimentally the situation has been studies for PBX-9404 in the case where an intense laser heated the inert material (stainless steel).

Eventhough the interface temperature rises above T_R, propagation does not begin immediately. Apparently a minimum extent of the HE (indicated in Figure 3 by d) needs to reach the temperature T_R before initiation propagation begins. It is hypothesized that the mobile reactants created in the narrow interface region quickly diffuse into the cold region and are not available for further reaction at the interface. When the point d attains the temperature T_R initiation begins. Analysis of the laser experiments for PBX-9404 indicates that this HE has a minimum length of the order of 0.1 cm; the particle beam experiments always had beam radii greater than this and thus a minimum radius requirement could not be observed.

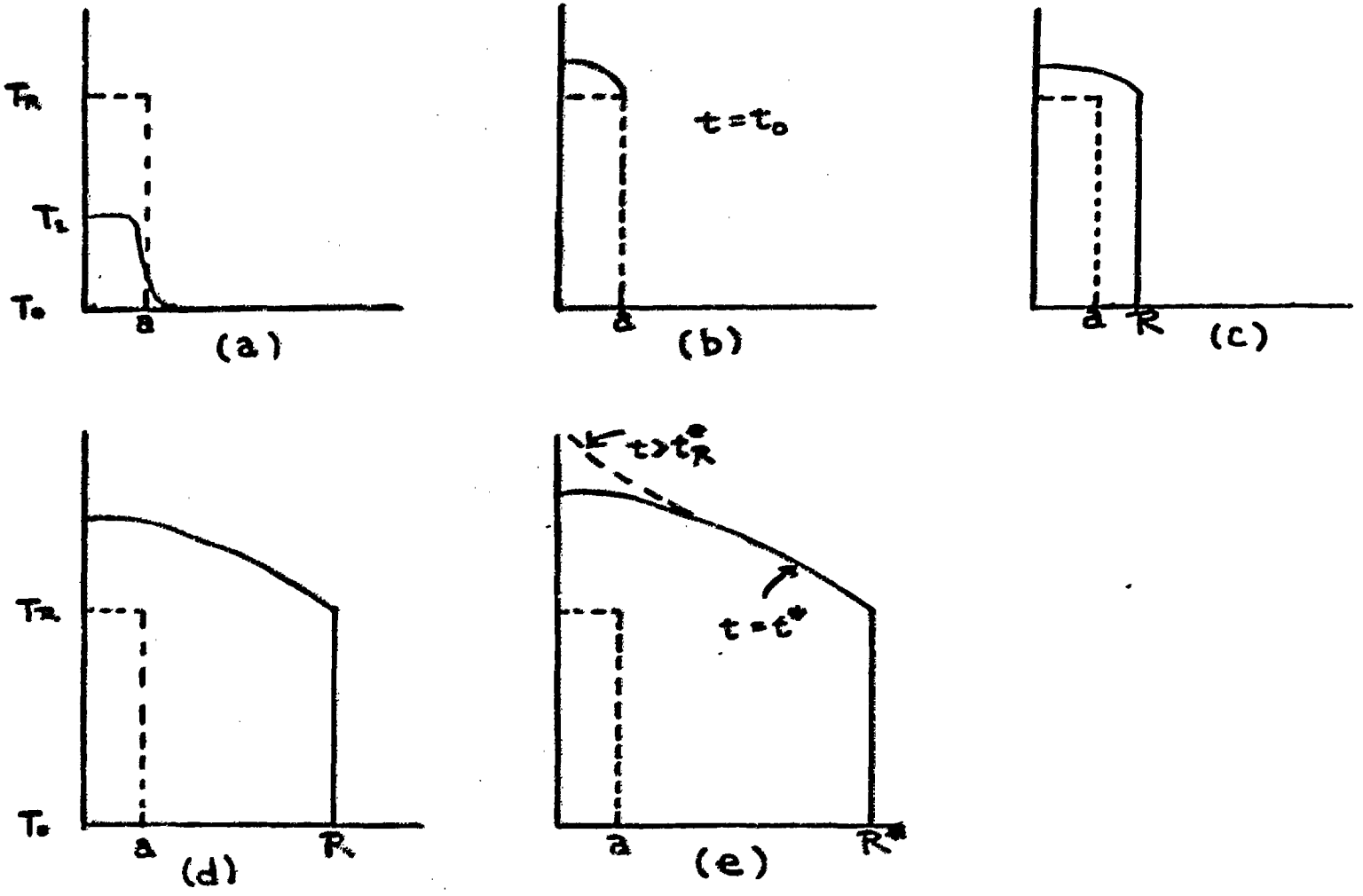

Figure 2

The concept present here and the analysis to follow only applies up to the time t^* when the front reaches the explosion radius R^*. What occurs afterward does so on a time scale less than a millisecond and depends on the material. The experiments described in Appendix A.1 indicate that for TATB no further reaction spreading occurs; for HBX-1 additional spreading occurs but does not consume the sample; for PBX-9404 additional spreading occurs and consumes the whole sample.

For the purpose of distinguishing thermal initiation propagation from DDT it is useful to describe a DDT model study for HMX made by Mader [Ref 3]. The geometry is planar and the extent of the HE is greater than 10 centimeters. The confinement is very strong in order to allow a deflagration started at one end of the HE to develop into a detonation wave ($c_o \sim 8 \times 10^5$ cm/sec) at the other end. In Mader's study modeling begins when several centimeters of the deflagrating end of the HE has reached kilobar range pressures; a detonation wave develops in about 20 microseconds. in the present study of thermal initiation propagation, the frontal motion is measured in milliseconds after initiation is first achieved in the beam region. Owing to the relatively weak confinement, the experiments were over (i.e., disruption occurred) when kilobar pressures were reached. Since the propagation time scale is much longer than the pressure relaxation time (~μ secs), isobaric conditions are maintained; large pressure excursions are judge only to occur near the time of disruption.

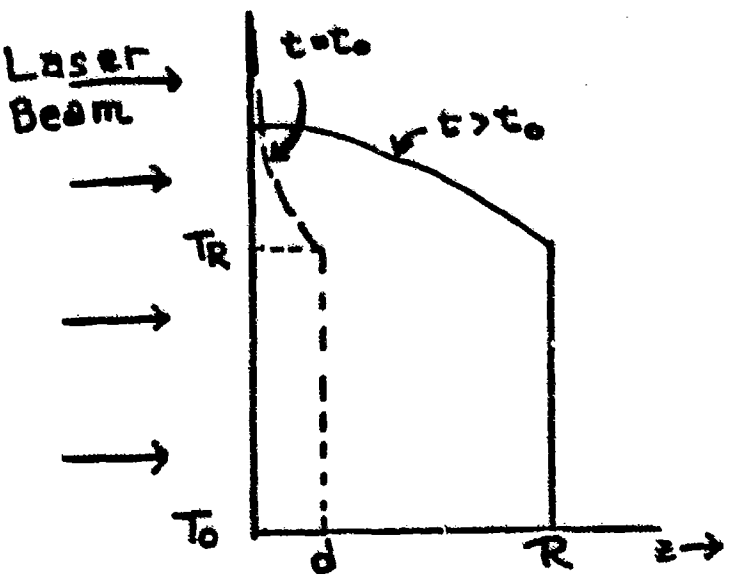

Figure 3

3. Exothermic Reaction Modeling

The microscopic chemical reactions which govern thermal explosions in condensed energetic materials are not fully known; even if they were, they would be too detailed for performance applications. In practice, calculations are often based on model reactions which utilize, as variables, the fraction N_A of molecules of the material which remains unreacted, and N_B the fraction that has reacted. The best models are based on actual experiments and have their limits of applicability defined.

The simplest model corresponds to unimolecular decomposition. The reaction scheme is

$$A \xrightarrow{k} B + A'; Q \tag{3.1}$$

The molecule A decomposes thermally, with rate constant k, into two (or more) different molecules and an amount of heat Q (per unit mass) is released. For a homogeneously reacting system the corresponding rate equation is

$$\frac{dN_A}{dt} = -k_A(T)N_A \tag{3.2}$$

The temperature dependence of the rate constant usually (though not always) takes the Arrhenius form:

$$k_A(T) = Z \exp(-T_A/T) \tag{3.3}$$

The pre-exponential factor Z has units of inverse seconds and T is the absolute temperature. The activation temperature is defined as follows:

$$T_A = E_A/R_g \tag{3.4}$$

where E_A is the activation energy (cal/mol) and R_g is the gas constant: $R_g = 1.987$ cal/mol-deg. The fraction of unreacted molecules is defined as

$$N_A = \frac{n_A}{n_o} \tag{3.5}$$

where n_o is the original number of molecules per unit volume and n_A is the number of molecules which are unreacted. The rate at which exothermic energy is released is

$$\frac{dq}{dt} = -Q\frac{dN_A}{dt} \tag{3.6}$$

in which q is the heat per unit mass acquired by the material.

A more detailed model corresponds to an autocatalytic scheme:

$$A \xrightarrow{k_A} B + A'; \; Q \tag{3.7a}$$

$$B + A \xrightarrow{k_B} B + B + A'; \; Q \tag{3.7b}$$

The molecule A decomposes into a molecule B and other products; then the molecule B reacts with other molecules A to produce a decomposition similar to the previous one, without itself changing. The first reaction occurs thermally, i.e., as a result of elevated temperature; the second is similar but occurs because of the presence of B which acts catalytically, i.e., it is not changed in the reaction. The corresponding rate equations are:

$$\frac{dN_A}{dt} = -k_A(T)N_A - k_B(T)N_A N_B \tag{3.8a}$$

$$\frac{dN_B}{dt} = k_A(T)N_A + k_B(T)N_A N_B \tag{3.8b}$$

in which

$$N_B = \frac{n_B}{n_o} \tag{3.9}$$

and n_B is the number of reacted molecules. It is convenient to introduce the notation

$$K(N_A, N_B; T) = k_A(T)N_A + k_B(T)N_A N_B \; . \tag{3.10}$$

The rate of heat generated per unit mass decomposed is

$$\frac{dq}{dt} = Q\frac{dN_B}{dt} = Q\,K(N_A, N_B; T) \; . \tag{3.11}$$

The reaction Eqs. (3.8 a, b) imply the following conservation relationship:

$$N_A + N_B = \text{const.} \tag{3.12}$$

If at the start of an experiment (t = 0) only type A is present, then

$$N_A(t=0) = 1 \; , \; N_B(t=0) = 0 \; , \tag{3.13}$$

thus

$$N_A = 1 - N_B \tag{3.14}$$

and

$$K = k_A(1 - N_B) + k_B(1 - N_B)N_B \tag{3.15}$$

Rogers, Janney, and co-workers [Ref. 4] have studied a large number of explosives by isothermal differential scanning calorimetry (DSC) and have analyzed their results with a generalized autocatalytic reaction scheme:

$$\frac{dN_B}{dt} = k_A(1 - N_B)^n + k_B(1 - N_B)^p N_B^q$$

They find that the exponents have the value unity, at least up to 50% decomposition, and in some cases beyond. Temperature variations yield reaction rates $k_A(T)$ and $k_B(T)$ that have the Arrhenius form over a wide temperature range; however the constants differ for each well defined region.

The temperature ranges studied by the DSC method except for TATB, do not go up to the thermal initiation temperature region investigated by Stolovy, et al. This is simply because the exothermic reaction rates become too large to hold the DSC system at constant temperature.

4. Adiabatic Thermal Initiation by Particle Beams

The thermal initiation of energetic materials by particle beams (electrons and protons) has been studied [Ref 1.] primarily in an adiabatic, homogeneous context with confinement. The material is uniformly irradiated by a particle beam which deposits energy uniformly at the rate $\dot{q}_b$ per unit mass. The pertinent equations are

$$\frac{dN_A}{dt} = -K(N_A, N_B; T) \tag{4.1a}$$

$$\frac{dN_B}{dt} = K(N_A, N_B; T) \tag{4.1 b}$$

$$\frac{dq}{dt} = C_V \frac{dT}{dt} = \dot{q}_b + QK(N_A, N_B; T) \tag{4.1c}$$

The equations imply

$$\frac{d(N_A + N_B)}{dt} = 0 \tag{4.2a}$$

$$C_V \frac{dT}{dt} - Q\frac{dN_B}{dt} = \dot{q}_b \tag{4.2b}$$

Integrating from room temperature ($t = 0$, $T = T_o$, $N_A(0)$) yields

$$N_A = 1 - N_B \tag{4.3a}$$

$$\int_{T_o}^{T} C_V \, dT - Q N_B = \dot{q}_b t \tag{4.3b}$$

The last equation simply states that difference between the internal energy and the decomposition energy is supplied by the beam energy deposition.

Experimentally, the temperature as a function of irradiation time is the primary data. Generic behavior is depicted in Figure 4:

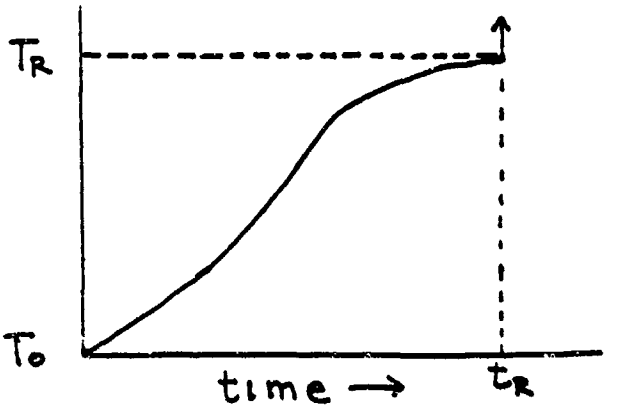

Figure 4

The initiation temperature is clearly indicated by the radical slope change at $T=T_R$. Below T_R, evidence for exothermic reactions is not very pronounced, while above T_R it is overwhelming. The amount of deposited beam energy required to bring the HE to initiation is called the initiation energy (from 25° C) and is denoted by E_R. Clearly

$$E_R = \dot{q}_b t_R \qquad \text{(from 25° C)} \qquad (4.4)$$

Extensive measurements of T_R and E_R have been made by Stolovy, et al [Ref 1]. For PBX-9404, whose propagation properties will be analyzed quantitatively in a later section, the values are

$$T_R = 280 \pm 5° \text{ C} \qquad (553 \pm 5° \text{ K})$$
$$E_R = 63.6 \pm 0.8 \text{ cal/gm} \qquad \text{(from 25° C)} \qquad (4.5)$$

The beam heating rate in these experiments varied between 7.62 and 11.28 cal/gm-sec, with an average at about 10 cal/gm-sec.

The detailed temperature behavior in the region around T_R, when looked at under high resolution, shows considerable variation from one HE material to another. For PBX-9404 the temperature achieves a plateau just before initiation; this indicates a phase change which is consistent with the known melting at 285°C. TATB exhibits a smooth, but rapid change at T_R = 409°C. The melt occurs at T_M = 450°C. The behavior of HBX-1, which consist of 40% RDX, 35% TNT and ~16% Al, is quite complex. Examples are given in Ref. 1.

Attempts to analytically understand thermal initiation by particle beams through use of reaction models with parameters taken from relatively low temperature thermal decomposition experiments have not been successful in reproducing the observed details in the vicinity above and below T_R. This would be explained if the reaction rate underwent a radical change at T_R. In this case the function of the particle beam is to (uniformly) bring the HE up to the temperature region where the radical change occurs. The initiation temperature

then is an intrinsic property of the HE. In what follows it will be seen, at least for PBX-9404, that the initiation front propagates with a temperature which is the same as the measured adiabatic initiation temperature, however the associated exothermic rate is several orders of magnitude higher than the beam rate ($\dot{q}_b$~10 cal/gm-sec) used in the adiabatic experiments. This lends support to the concept of a radical change occurring at a temperature T_R which is intrinsic to the materials.

For analysis of propagation the reaction rate needs to be known in a temperature region $\lesssim$ 40°C above the initiation temperature T_R. The following form will be used

$$KQ \cong \dot{q}_R \exp\left[\frac{T_\alpha}{T_R^2}(T - T_R)\right] \tag{4.6}$$

in which $\dot{q}_R$ is the exothermic rate at initiation and T_α is an effective activation temperature. In Appendix A.2 it is shown that the autocatalytic reaction rate Eq. 3.10, with $k_A(T)$ and $k_B(T)$ in the Arrhenius form, assume the form in Eq (4.6) for a limited temperature range. For given reaction constants in Eq. 3.10, Z_A, Z_B, T_A, T_B, the quantities $\dot{q}_R$ and T_α can be determined; lacking the former, the latter quantities must be treated as model parameter to be determined by comparison with experiment. The value of the initiation energy and temperature from adiabatic experiments are important parameters entering into the propagation equation.

5. Simple Model for Initiation Propagation

In order to fix notions for the dynamics of the moving front it is useful to construct a simple model: it is assumed that diffusion is small for $T < T_R$ and that heat transport, by any means, is very large for $T > T_R$. Once initiation propagation begins, the temperature in the initiated region remains constant since all of the newly generated energy moves immediately to the cold region. Figure 5 illustrates the model situation.

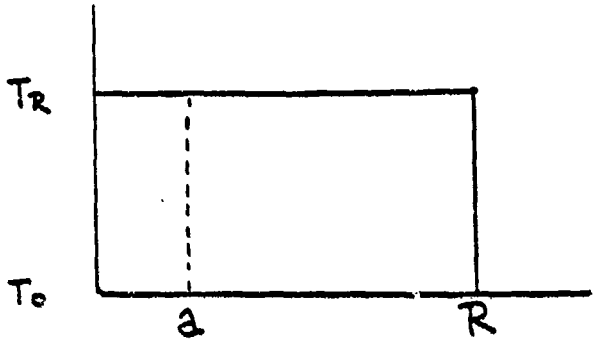

Figure 5

As a matter of convenience, the beam is turned off once initiation is achieved. The energy increment of the initiated region is

$$U - U_o = E_R M_R \tag{5.1}$$

Where M_R is the mass of the initiated region and E_R is the energy per unit mass required to take the material from T_o to T_R. The experimentally measured initiation energy will be used in calculations. The rate at which energy changes in the initiated region is given by

$$\frac{dU}{dt} = \dot{q}_R M_R \tag{5.2}$$

in which $\dot{q}_R$ is the rate of change of energy per unit mass. This quantity is not assumed to be the same as the beam energy rate which produced initiation. Both $\dot{q}_R$ and T_R are quantities established when initiation spreading occurs.

Energy conservation requires

$$\frac{dU}{dt} = \dot{q}_R M_R = E_R \frac{dM_R}{dt} \tag{5.3}$$

For cylindrical geometry, with R = radius and l = length,

$$M = \pi R^2 l \mu \tag{5.4}$$

where μ is the mass density. Equation (5.3) reduces to

$$\frac{\dot{q}_R}{E_R} = \frac{2}{R}\frac{dR}{dt} \tag{5.5}$$

The time constant $t_1 = E_R/\dot{q}_R$ is the time required to adiabatically change the energy of a unit mass of the material by an amount E_R if the heating rate is $\dot{q}_R$. The solution to Equation (5.5) is

$$\frac{t}{t_1} = 2 \ln \frac{R}{a} \tag{5.6}$$

in which it is assumed that propagation begins at point a at time t = 0. This relation will now be applied to the PBX-9404 data found in the appendix and repeated here:

$$\begin{array}{lll} a_{coll} = 0.238 \text{ cm} & & \text{(collimation radius)} \\ R_1 = 0.476 \text{ cm} & t_1 = 25.0 \text{ msec} & \\ R_2 = 0.953 \text{ cm} & t_2 = 43.8 \text{ msec} & \end{array} \tag{5.7}$$

Assuming that propagation begins at the collimation radius, the data at position 2 gives

$$t_1 = \frac{t_2}{2 \ln (R_2/a_{coll})} = 15.8 \text{ msec} \tag{5.8}$$

Alternatively, the use of the information at the two positions gives

$$t_1 = \frac{(t_2 - t_1)}{2} \frac{1}{\ln (R_2/R_1)} = 13.5 \text{ msec}$$

$$\ln a = \ln R_2 - \frac{1}{2}\frac{t_2}{t_1} = -1.67 \tag{5.9}$$

$$a = 0.188 \text{ cm} \qquad \text{(model value)}$$

The values obtained have about a 20% uncertainty.

If now the experimental value $E_R = 64$ cal/gm is used, then

$$\dot{q}_R = \frac{E_R}{t_I} = 4.74 \times 10^3 \text{ cal/gm–sec} \qquad (5.10)$$

The large magnitude of this value relative to the beam heating rate (~ 10 cal/gm-sec) is not changed by subsequent refinements in the analysis. It is simply the minimum rate at which exothermic energy must be generated in order to produce a front with the observed motion.

The data in Equation (5.7) indicate that the explosion time after initiation has occurred is something in excess of 44 msec. It is instructive to compare this to the explosion time in the adiabatic case, i.e., no propagation. A simplified exothermic heating rate model equation is (see Section 4):

$$C_V \frac{dT}{dt} = \dot{q}_R \exp\left[\frac{T_\alpha}{T_R^2}(T - T_R)\right] \qquad (5.11)$$

The time to explosion, i.e., the time it takes for the temperature to go from T_R to ∞, is given by

$$t_e = \frac{C_V}{\dot{q}_R}\int_{T_R}^{\infty} \exp\left[-\frac{T_\alpha}{T_R^2}(T - T_R)\right] dT = \frac{C_V}{\dot{q}_R}\frac{T_R^2}{T_\alpha} \qquad (5.12)$$

For PBX-9404, a standard value of T_α and C_v are

$$T_\alpha \cong 26{,}000^\circ \text{K}$$

$$C_v \cong 0.4 \text{ cal/gm} \qquad \text{(high temp.)} \qquad (5.13)$$

These give, with the experimental $T_R \cong 553^\circ$ K,

$$t_e \cong 1 \text{ msec} \qquad (5.14)$$

Thus the actual explosion time, after initiation, is increased by more than an order of magnitude as a result of propagation.

It is also instructive to calculate the fraction of the original material which must decompose in order to generate the energy that keeps the front moving. this is given by

$$\frac{\Delta M}{M} = \frac{E_R}{Q} \qquad (5.15)$$

in which Q is the exothermic energy per unit mass decomposed and E_R, the

initiation energy, is the energy required to bring the cold material at the front to the initiation temperature T_R. The extreme values of Q, for PBX-9404, are given as

$$Q \equiv \left\{ \begin{matrix} 500 \text{ cal/gm} & \text{(Thermal Explosion)} \\ 1500 \text{ cal/gm} & \text{(Detonation)} \end{matrix} \right\} \tag{5.16}$$

Since $E_R = 64$ cal/gm, the above yields

$$.04 \lesssim \frac{\Delta M}{M} \lesssim 0.13 \tag{5.17}$$

Thus, the order of 10% of the available exothermic energy is expended on propagation; the remainder will go into the final explosion when it occurs.

The main failing in the simple model considered here is that propagation is unlimited. Inversion of Equation (5.6) yields

$$R(t) = a \exp(t/2\, t_l) \tag{5.18}$$

The more elaborate model to follow, in which finite diffusivity and mass flow is accounted for, contains naturally a limiting radius R^* at which an explosion will occur. For finite diffusivity there will always be a point at which all the energy generated in the vicinity of $R = 0$, cannot diffuse to the front. The temperature in the central region will then rise and, owing to the autoaccelerating nature of the reactions rate, will quickly destablize the quasi-equilibrium state essential for propagation. For PBX-9404, the value of R^* will be a centimeter. However the value of the diffusivity will be $\sim 10^3$ cm^2/sec. Owing to this very large diffusivity, the values of t_l, a, and $\dot{q}_R$ obtained in the simple model are very nearly correct; only the extent of propagation is modified. The extent of propagation, R^*, is very important since it determines the minimum amount of HE which will undergo thermal explosion.

6. General Transport Theory and Modeling

In this section general transport equations and concepts will be developed. The general analysis techniques are based on Landau and Lifschitz's "Fluid Mechanics"[Ref. 5]. Thermal initiation propagation modeling, based on experimental observations, will be then performed.

The basic conservation/generation equation has the general form:

$$\frac{\partial \phi}{\partial t} + \nabla \cdot \vec{j_\phi} = S_\phi \qquad (6.1)$$

in which ϕ is a density (e.g., mass, momentum component, energy, etc., per unit volume); $\vec{j_\phi}$ is the corresponding flux vector. If S_ϕ vanishes, and if $\vec{j_\phi}$ vanishes at the boundary of the space under consideration, then

$$\int \phi \, d\upsilon = \text{const.} \qquad (6.2)$$

i.e. the total amount of the quantity in the volume υ is conserved. When a quantity is not conserved its rate of generation per unit volume is specified by the source term S_ϕ.

The HE material is assumed porous. When the initiation temperature, T_R, is reached the material decomposes exothermically and produces solid and gaseous products. Physical changes in the solid substrate may precipitate initiation. Hot gases, filling the pores, produce increasing pressure which, if not relieved, will produce an explosion in less than a millisecond. Relief can be obtained by heat conduction and mass flow out of the initiated region into the cold uninitiated region. Since pressure relaxation takes place on a time scale much shorter than the observed initiation propagation time, pressure wave propagation will not be significant until the explosion occurs. Mass transport of the gaseous products through the porous material will be allowed for. General thermal conduction is taken into account and will be shown to dominate.

The thermal initiation propagation model to be developed is meant to apply from the time when the initiation temperature is reached until the time when the quasi-steady state propagation can no longer be maintained. At this latter time rapid temperature and pressure changes begin and an explosion develops on a millisecond time scale.

Specific reaction modeling will be a generalization of the autocatalytic reaction process to include energy and mass transport. For convenience the process is repeated here:

$$A \rightarrow B + A'$$
$$B + A \rightarrow 2B + A' \qquad (6.3)$$

The product B is assumed to be a gas and A' is assumed to be a solid (or at least an immobile liquid).

A microscopic description of the phenomena to be modeled is not available. It is thus appropriate to take as the elementary material "point" a small macroscopic volume which contains many pores. The motion of the gas within the elementary "point" is locally convective and highly chaotic. No attempt will be made to model behavior within the "point". The average properties over the small macroscopic volume will be used. These will either be inferred from experiment or postulated by reasonable argument.

For each component i = A, A', B the number per unit volume is designated by n_i; the initial value of n_A is n_o. It continues to be convenient to express numbers of molecules as fractions of the initial number of type A:

$$N_i = \frac{n_i}{n_o} \qquad (6.4)$$

The two solid components, A and A', and their molecular masses are related as follows:

$$n_{A'} = n_o - n_A$$
$$m_{A'} = m_A - m_B \qquad (6.5)$$

Through these relations any explicit dependence on A' can be removed. It should be noted that

$$n_{A'} \neq n_B \qquad (6.6)$$

since B is free to move from its place of origin, whereas A' is not

Although number density is most convenient in discussing reactions, mass density must be introduced for hydrodynamics. The following relations, for mass density μ_i, hold:

$$\mu_i = m_i n_i = \frac{m_i}{m_A} \mu_o N_i \qquad (6.7)$$

where

$$\mu_o = m_A n_o \qquad (6.8)$$

The total solid density is

$$\mu_s = \mu_A + \mu_{A'} \tag{6.9}$$

and

$$d\,\mu_s = \frac{m_B}{m_A}\mu_o\, d\,N_A \tag{6.10}$$

The fractional volume occupied by the pores is defined as

$$\sigma = \frac{\upsilon_{pores}}{\upsilon} \tag{6.11}$$

where υ is the total volume. The quantity is assumed not to change significantly in the initiated region during the quasi-steady state propagation period. The average macroscopic gas density μ_B is related to the true average gas density, ρ_B, in the pores by

$$\mu_B = \sigma\,\rho_B \tag{6.12}$$

The fundamental kinematic variable is the average mass flow velocity $\vec{V}$ which is defined as the average gas momentum per unit gas mass. The momentum per unit macroscopic volume is then given by $\mu_B\vec{V}$. The mass conservation/generation equation for B is then

$$\frac{\partial \mu_B}{\partial t} + \nabla \cdot \mu_B\vec{V} = \mu_o\mathcal{R} \tag{6.13}$$

in which $\mu_o\mathcal{R}$ is the rate of generation (per unit macroscopic volume) of gaseous mass which results from reactions in or with the solid substrate. It follows that

$$\frac{\partial N_B}{\partial t} + \nabla \cdot N_B\vec{V} = \frac{m_A}{m_B}\mathcal{R} \tag{6.14}$$

In Section 3 the reaction rate for N_B was designated by $\mathcal{K}$, thus

$$\mathcal{R} = \frac{m_B}{m_A}\mathcal{K} \tag{6.15}$$

For the solid components, neither of which move,

$$-\frac{\partial N_{A'}}{\partial t} = \frac{\partial N_A}{\partial t} = -\mathcal{K} \tag{6.16}$$

and

$$\frac{\partial \mu_s}{\partial t} = \mu_o \bar{K} \tag{6.17}$$

Turning now to momentum transfer, which by previous assumption (i.e., no pressure waves in the solid) will only involve the gas, the conservation/generation equation is (neglecting internal gas viscosity)

$$\frac{\partial \mu_B \vec{V}}{\partial t} + \nabla \cdot \left(\mu_B \vec{V}\vec{V} + \bar{P}\bar{1}\right) = \mu_B \vec{f} \tag{6.18}$$

in which P is a pressure and $\bar{1}$ is the unit tensor. This equation is first obtained in terms of the true density and pressure in the pores, ρ_B and P, and then multiplied by σ. Thus

$$\bar{P} = \sigma P \tag{6.19}$$

The only source (actually a sink) of gas momentum is the reduction of the flow momentum through interaction with the porous substrate. The force per unit mass, $\vec{f}$, results from viscous effects and flow randomization that occur within the material "point"; it is reasonably (and usually) modeled by

$$\vec{f} = -\Omega \vec{V} \tag{6.20}$$

in which Ω, the flow resistance, will be assumed constant during the propagation period.

Eq. (6.13) implies the following identity for an arbitrary quantity G:

$$\frac{\partial \mu_B G}{\partial t} + \nabla \cdot \left(\mu_g G \vec{V}\right) = \mu_B \frac{dG}{dt} + \mu_o \bar{K} G \tag{6.21}$$

in which

$$\frac{d}{dt} = \frac{\partial}{\partial t} + \vec{V} \cdot \nabla \tag{6.22}$$

Setting $G = \vec{V}$ in Eq. (6.21) and combining the result with Eq. (6.18) results in

$$\mu_B \frac{d\vec{V}}{dt} = -\nabla P + \mu_B \vec{f} - \mu_o \bar{K} \vec{V} \tag{6.23}$$

Although the generation of gas (which has zero average velocity) is not a source of momentum, the newly generated gas acquires momentum from the flowing

gas; this causes a reduction in the average velocity which is accounted for by the last term in Eq. (6.23).

In making energy consideration, the system as a whole is taken as closed, i.e., no energy is introduced from the outside; the beam has either been turned off, or (as was seen in Section 5) the beam energy deposition rate is negligible compared to the reaction energy rate. The conservation equation for the system as a whole, i.e., solid plus gas, is

$$\frac{\partial(\mu_S \varepsilon_S)}{\partial t} + \frac{\partial}{\partial t}\mu_B\left(\varepsilon_B + \frac{1}{2}\vec{V}^2\right) + \nabla\cdot\left[\mu_B \vec{V}\left(h_B + \frac{1}{2}\vec{V}^2\right) + \vec{q}\right] = 0 \qquad (6.24)$$

in which ε_S and ε_B are the solid and gaseous energies per unit mass, and

$$h_B = \varepsilon_B + \frac{\bar{P}}{\mu_B} = \varepsilon_B + \frac{P}{\rho_B} \qquad (6.25)$$

is the enthalpy per unit mass of the gas. The heat flux vector $\vec{q}$ accounts for any energy transport that is not associated with mass transport.

Several transformation will now be made which will make internal heating effects (and entropy transport) explicit. First apply Eq. (6.21) with $G = h_B + \frac{1}{2}\vec{V}^2$. When combined with Eq. (6.24) this results in

$$\frac{\partial(\mu_S \varepsilon_S)}{\partial t} + \mu_B \frac{dh_B}{dt} - \frac{\partial \bar{P}}{\partial t} + \mu_B \frac{d}{dt}\left(\frac{1}{2}\vec{V}^2\right) + \mu_o K\left(h_B + \frac{1}{2}\vec{V}^2\right) + \nabla\cdot\vec{q} = 0 \qquad (6.26)$$

Next , take the scalar product of $\vec{V}$ with eq. (6.23). The result is

$$\mu_B \frac{d\left(\frac{1}{2}\vec{V}^2\right)}{dt} = -\vec{V}\cdot\nabla\bar{P} + \mu_B \vec{V}\cdot\vec{f} - \mu_o K \vec{V}^2 \qquad (6.27)$$

Inserting this into Eq. (6.26) yields

$$\frac{\partial(\mu_S \varepsilon_S)}{\partial t} + \mu_B \frac{dh_B}{dt} - \frac{d\bar{P}}{dt} + \mu_B \vec{V}\cdot\vec{f} - \mu_o K \vec{V}^2 + \mu_o K\left(h_B + \frac{1}{2}\vec{V}^2\right) + \nabla\cdot\vec{q} = 0 \qquad (6.28)$$

Utilization will now be made of the following thermodynamic relations which hold for either the solid or the gaseous component:

$$d\varepsilon_i = T\,d\,s_i + \frac{\bar{P}}{\mu_i^2}\,d\mu_i \qquad (6.29a)$$

$$dh_i = T\,d\,s_i + \frac{dP}{\mu_i} \tag{6.29b}$$

$$d(\mu_i \varepsilon_i) = \mu_i\, T\, d\, s_i + h_i\, d\mu_i \tag{6.29c}$$

in which s_i is the entropy per unit mass of the i^{th} component. Introducing these into Eq. (6.28) results in

$$\begin{aligned} \mu_s T \frac{\partial s_S}{\partial t} + \mu_B T\left(\frac{\partial s_B}{\partial t} + \vec{V}\cdot\nabla s_B\right) &= \mu_o R\left(h_s - h_B - \frac{1}{2}\vec{V}^2\right) \\ -\mu_B \vec{V}\cdot\left(\vec{f} - \frac{\mu_o}{\mu_B} R\,\vec{V}\right) - \nabla\cdot\vec{q} &= 0 \end{aligned} \tag{6.30}$$

This is the general equation of heat transfer for the solid-gas system undergoing exothermic reactions. The first term on the left is the rate of heating (per unit volume) of the solid; the second term is the rate of heating of the moving gas. The right hand side exhibits the internal sources of heat: The first term results from decomposition with the non-heating kinetic energy subtracted off; the second term is the heating rate produced by the dissipation of kinetic energy of the flowing gas as a result of the interaction with the porous solid substrate and the newly created (zero-velocity) gas; the last term arises from thermal conduction. The decomposition term can be written in terms of the heat of reaction as follows:

$$\mu_o R\left(h_s - h_B - \frac{1}{2}\vec{V}^2\right) = \mu_o K\left(Q - \frac{m_B}{2\,m_A} V^2\right) \tag{6.31}$$

where

$$Q = \frac{m_B}{m_A}(h_s - h_B) \tag{6.32}$$

The heat flux vector, on general grounds, is taken to be

$$\vec{q} = -\kappa\nabla T \tag{6.33}$$

The thermal conductivity κ is assumed not to vary significantly for the quasi-steady state variation to be considered $(\Delta T \lesssim 40^\circ C)$. The heating rates, as usual, are written

$$T\frac{\partial s_i}{\partial t} = T\frac{\partial s_i}{\partial T}\frac{\partial T}{\partial t} = c_i\frac{\partial T}{\partial t} \tag{6.34}$$

in which c_i is an appropriate specific heat. A detailed analysis is not in order; it will suffice to write

$$\mu_s T \frac{\partial s_s}{\partial t} + \mu_B T \frac{\partial s_B}{\partial t} = \mu \bar{c}_v \frac{\partial T}{\partial t} \tag{6.35}$$

where

$$\bar{c}_v \equiv \frac{\mu_s c_s + \mu_B c_B}{\mu_s + \mu_B} \tag{6.36}$$

is an effective specific heat and

$$\mu = \mu_s + \mu_B \tag{6.37}$$

is the total mass density. Whenever a value for $\bar{c}_v$ is needed, an estimated high temperature value for the unreacted HE (the dominant component) will be used. Eq. (6.30) can now be written

$$\begin{aligned} \mu \bar{c}_v \frac{\partial T}{\partial t} + \mu_B T \vec{V} \cdot \nabla s_B &= \mu_o K \left(Q - \frac{m_B}{2 m_A} \vec{V}^2 \right) \\ - \mu_B \vec{V} \cdot \left(\vec{f} - \frac{\mu_o m_B}{\mu_B m_A} K \vec{V} \right) - \nabla \cdot \vec{q} &= 0 \end{aligned} \tag{6.38}$$

Having now established sufficiently general equations governing mass, energy, and momentum transfer for the system, the analysis will now turn to comparing the roles of mass flow and heat conduction in transporting energy toward the cold region during the quasi-steady state thermal initiation propagation. Of necessity, the analysis is done specifically for PBX-9404, however general conditions are stated so that applications will be facilitated whenever sufficient information is available for other HE materials.

The main factors to be used are:

1. The flow velocity must not be greater than the initiation front velocity. Then

$$V < 50 \text{ cm/sec} \tag{6.39a}$$

$$1/2\, V^2 < 1.25 \times 10^3 \text{ ergs/gm} \tag{6.39b}$$

This factor has already been used to rule out sound (i.e. pressure) propagation. The solid components are considered mechanically rigid.

2. The heat of reaction is quite large:

$$Q \sim 500 - 1500 \text{ cal/gm}$$

(6.40)

$$\sim 2 \times 10^{10} - 6 \times 10^{10} \text{ ergs/gm}$$

Since, in the sample model of Section 5, the rate of heat production was deduced to be quite high, the larger possible values of Q are favored. A value of Q = 1000 cal/gm = 4×10^{10} ergs/gm will be used in estimates

3. The rate of increase of the heat in the initiated region during the propagation period must be considerably less than the exothermic reaction energy rate:

$$\mu c_v \frac{\partial T}{\partial t} << \mu_o Q K \tag{6.41a}$$

If this did not hold, an autoaccelerating temperature increase would bring about an explosion.

A fundamental conclusion is arrived at by looking at Eq. (6.38) in the vicinity of the center of cylinder (r = 0). Since the mass flux must vanish here, the velocity also vanishes. Thus Eq. (6.38) reduces to

$$\mu c_v \frac{\partial T}{\partial t} + \nabla \cdot \vec{q} = \mu_o K Q \tag{6.41b}$$

Eq. (6.41a) then implies that thermal conduction dominates the region about the origin. Using Eq. (6.33), Eq. (6.41b) can be written

$$\frac{\partial T}{\partial t} - D_T' \nabla^2 T = \frac{\mu_o}{\mu} \frac{Q}{c_v} K \tag{6.41c}$$

where

$$D_T' = \frac{\kappa}{\mu c_v} \tag{6.41d}$$

is the thermal diffusivity (units = cm^2/sec). Once initiation is achieved in the beam region, an explosion can be prevented by thermal conduction if the heat diffuses out of the beam region ($r \leq a$) on the time scale t_s = 1 msec for an adiabatic explosion. This gives

$$\sqrt{D_T' t_s} > a \tag{6.41e}$$

or

$$D_T' > .25 \times 10^{-3} \text{ cm}^2/\text{sec}.$$

Thus a very large thermal diffusivity is anticipated.

In due course all velocity dependent terms in Eq. (6.38) will be analyzed. To begin with, Eqs. (6.39b) and (6.40) imply.

$$\tfrac{1}{2}\frac{m_B}{m_A}V^2 << Q \tag{6.42}$$

Thus Eq. (6.38) becomes

$$\mu \bar{c}_v \frac{\partial T}{\partial t} + \mu_B T \vec{V} \cdot \nabla s_B + \nabla \cdot \vec{q} = \mu_o KQ - \mu_B \vec{V} \cdot f \tag{6.43}$$

Further reduction will come after consideration of the momentum transport.

For one-dimensional flow, the momentum flux contained in Eq. (6.18) is

$$j_{mom} = \mu_B\left(V^2 + \frac{\bar{P}}{\mu_B}\right) \tag{6.44}$$

The gas will be assumed to be ideal. Thus

$$\bar{P} = \alpha n_B k T \tag{6.45a}$$

If the product B is a single molecule then $\alpha = 1$. If the product consist of α molecules, their partial pressure add up to give Eq. (6.45a). It is assumed that the relative concentrations do not change during propagation. Introducing mass densities yields.

$$\frac{\bar{P}}{\mu_B} = \alpha \frac{R_g}{M_B} T \tag{6.45b}$$

In which $R_g = 8.3 \times 10^7$ ergs./mol-deg (gas constant). Since $T > 553°$ ($=T_R$) and the average molecular weight $M_B/\alpha < 300$ gms/mol (HMX), the following holds:

$$\frac{\bar{P}}{\mu_B} > 1.5 \times 10^8 \text{ cm}^2/\text{sec}^2 >> V^2 \tag{6.46}$$

Using this result and Eq. (6.20), Eq. (6.18) becomes

$$\frac{\partial \mu_B \vec{V}}{\partial t} + \Omega \mu_B \vec{V} = -\nabla \bar{P} \tag{6.47}$$

This equation is formally solved as follows:

$$\mu_B \vec{V} = \mu_B \vec{V} \Big/_{t=t_1} e^{-\Omega(t-t_1)} - e^{-\Omega(t-t_1)} \int_{t_1}^{t} e^{\Omega(t'-t_1)} \nabla \bar{P}\, dt' \qquad (6.48a)$$

Repeated integration by parts yields

$$\mu_B \vec{V} = \mu_B \vec{V} \Big/_{t_1} e^{-\Omega(t-t_1)} - \nabla\left(\frac{\bar{P}}{\Omega} - \frac{1}{\Omega^2} \frac{\partial \bar{P}}{\partial t} + O\left(\frac{1}{\Omega^3}\right)\right) \qquad (6,48b)$$

For a sufficiently large flow resistance Ω. Eq. (6.48) reduces to

$$\mu_B \vec{V} = - \frac{\nabla \bar{P}}{\Omega} \qquad (6.49)$$

Thus, in a time interval

$$\Delta t_f \sim \Omega^{-1} \qquad (6.50)$$

The mass flux relaxes to a quasi-steady state value given by Eq. (6.49). Once the rate of pressure increase becomes explosively large this situation is terminated.

The flow resistance Ω is the primary parameter determining the mass flow. Unfortunately, the experiments do not give any measure of mass flow. The frontal velocity, which marks the progress of initiation, gives only a possible upper bound Despite this uncertainty, a useful lower bound to Ω can be conjectured as follows: It is reasonable to assume that the drag force due to the porous material is much greater than the drag force due to the creation of zero (average) velocity gas.

Thus, from Eq. (6.23),

$$\mu_B \vec{f} = \Omega \mu_o \vec{V} >> \mu_o K \vec{V} = \mu_o \frac{m_B}{m_A} K \vec{V} \qquad (6.51a)$$

or

$$\Omega >> \frac{K}{N_B} \qquad (6.51b)$$

From the simple model presented in Section 5,

$$K = \frac{\dot{q}_R}{Q} \qquad (6.52a)$$

$$\frac{\Delta M}{M} = N_B,\ N_B Q \equiv E_R \tag{6.52b}$$

Thus

$$\Omega >> \frac{\dot{q}_R}{E_R} = \frac{1}{t_l} \tag{6.53a}$$

or

$$\Omega^{-1} \equiv \Delta t_f << t_l = 12 \text{ msec} \tag{6.53b}$$

Thus a flow relaxation time of the order of a millisecond is not unreasonable and assures that the quasi-steady form given by Eq. (6.49) holds during the propagation period which lasts about 40 msecs.

Eq. (6.49) now replace the momentum equation. The mass and energy equations now take the form

$$\frac{\partial \mu_B}{\partial t} - \frac{1}{\Omega} \nabla^2 \bar{P} = \mu_o \frac{m_B}{m_A} K \tag{6.54}$$

$$\mu \bar{c_v} \frac{\partial T}{\partial t} + \mu_B \vec{V} \cdot \left(T \nabla s_B + \frac{\nabla P}{\mu_B} \right) + \nabla \cdot \vec{q} = \mu_o Q R \tag{6.55}$$

The effort will now be directed toward deriving conditions under which the velocity dependent term in Eq. (6.55) can be neglected relative to the conduction term. Applying Eq. (6.29b) to the present situation.

$$T \nabla s_B + \frac{\nabla \bar{P}}{\mu_B} = \nabla h_B \tag{6.56}$$

For an ideal gas, in a limited temperature range,

$$d h \equiv c_p d T \tag{6.57}$$

thus,

$$\mu \bar{c_v} \frac{\partial T}{\partial t} + \mu_B \vec{V} \cdot c_{pB} \nabla T + \nabla \cdot q = \mu_o K Q \tag{6.58}$$

Reintroducing $\vec{q} = -\kappa \nabla T$, and redefining a thermal diffusivity

$$D_T = \frac{\kappa}{\mu_o \bar{c_v}}$$

Eq. (6.58) becomes

$$\mu \tilde{c}_v \frac{\partial T}{\partial t} - \frac{\mu_B}{\mu_o} \frac{c_{pB}}{\tilde{c}_v} \frac{\vec{V} \cdot \vec{q}}{D_T} + \nabla \cdot \vec{q} = \mu_o K Q \tag{6.58}$$

Appropriately neglecting the time derivative, a formal solution of eq. (6.58), for $\vec{q}$, is (in cylindrical coordinates):

$$r q = e^{\nu r} \int_o^r e^{-\nu r'} \mu_o K Q r' d r' \tag{6.59}$$

where

$$\nu = \frac{\mu_B}{\mu_o} \frac{c_{pB}}{\tilde{c}_v} \frac{V}{D_T} \tag{6.60}$$

If the exponential in Eq. (6.59) are essentially unity, the velocity dependent term in Eq. (6.58) is negligible. This requires

$$\nu r << 1 \tag{6.61a}$$

or

$$D_T >> \frac{\mu_B}{\mu_o} \frac{c_{pB}}{\tilde{c}_v} V r \tag{6.61b}$$

The maximum r is about 1 cm., the maximum v ~ 50 cm/sec. The following is considered reasonable.

$$.01 < \frac{\mu_B}{\mu_o} \frac{c_{pB}}{\tilde{c}_v} < 1 \tag{6.62}$$

Conservatively then,

$$D_T > > 50 \text{ cm}^2/\text{sec} \tag{6.63}$$

is a sufficient condition for neglecting the velocity dependent term in Eq. (6.58). Comparing this with Eq. (6.41e) (with $\mu \sim \mu_o$) shows that Eq. (6.63) holds quite adequately.

It is now appropriate to gather the complete set of properly reduced equations which determine N_A, N_B, P, $\vec{V}$, and T:

From Eq. (6.16)

$$\frac{\partial N_A}{\partial t} = -K \tag{6.64}$$

From Eq. (6.54)

$$\frac{\partial N_B}{\partial t} - \frac{D_N}{T_R} \nabla^2 (N_B T) = K \tag{6.65a}$$

Here, the pressure in the form (from Eq. (6.45b))

$$\bar{P} = \alpha \mu_B \frac{R_g}{M_B} T = \alpha \frac{m_B}{m_A} \mu_o \frac{R_g}{M_B} N_B T \tag{6.65a}$$

has been used. Most directly,

$$\bar{P} = \alpha \mu_o \frac{R_g}{M_A} N_B T \tag{6.65b}$$

Also, a diffusion coefficient D_N has been defined:

$$D_N = \alpha \frac{R_g T_R}{M_B} \frac{1}{\Omega} \tag{6.66}$$

From Eq. (6.49)

$$N_B \vec{V} = -\frac{D_N}{T_R} \nabla (N_B T) \tag{6.67}$$

From Eq. (6.58)

$$\frac{\mu}{\mu_o} \frac{\partial T}{\partial t} - D_T \nabla^2 T = \frac{Q}{\bar{c}_v} K \tag{6.68a}$$

where

$$D_T = \frac{\kappa}{\mu_o \bar{c}_v} \tag{6.68b}$$

The development in this section have not depended on a specific form for the reaction rate. Most generally.

$$K = K(N_A, N_B; T) \tag{6.69}$$

An alternate version to Eq. (6.65a) is

$$\frac{\partial (N_B T)}{\partial t} - \frac{T}{T_R} D_N \nabla^2 (N_B T) = T K + N_B \frac{\partial T}{\partial t} \tag{6.70}$$

By Eq. (6.41a)

$$N_B \frac{\partial T}{\partial t} << \frac{N_B Q}{\bar{c}_v} K \approx \frac{E_R}{\bar{c}_v} K \tag{6.70a}$$

Thus the last term on the right of Eq. (6.70) can be neglected during propagation. The result is

$$\frac{\partial (N_B T)}{\partial t} - D_P \nabla^2 (N_B T) = T K \tag{6.71}$$

This is a diffusion equation for the pressure with source = TK and diffusivity

$$D_P = \frac{R_g T}{(M_B/\alpha)} \frac{1}{\bar{\Omega}} \tag{6.72}$$

Neither experiments nor the present macroscopic analysis can give an estimate for D_P. It will be assumed that D_P is not greater than D_T; this implies that not much is going on in the cold material before the approach of the initiation front. This is consistent with the previous assumption that the mass flow velocity can not exceed the frontal velocity. If the flow resistance is sufficiently great, D_P could be considerable less than D_T.

The last topic to be covered in this section is the boundary and initial conditions that must be satisfied by the closed set of equations given by Eqs. (6.64), (6.65a), and (6.68a) for N_A, N_B, and T. These are of the form

$$\frac{\partial \phi}{\partial t} + \nabla \cdot \vec{j}_\phi = S_\phi \tag{6.73}$$

Only the particle beam case (in cylindrical symmetry) will be analyzed completely. The following sketch for $\phi = N_B$ or T is useful.

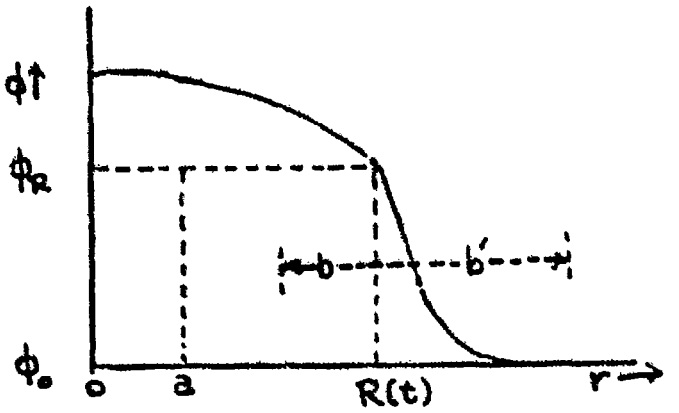

The initiation front is the (cylindrical) surface over which the temperature is T_R

and is designated by the radial distance R(t) which is changing at the rate dR/dt. At r = R(t), N_B and T are continuous, however they are expected to diminish very sharply in regions II owing to a drop in diffusivity. The fluxes are continuous but a discontinuity in the diffusivities implies a discontinuity in the gradients at r = R(t).

Since Eq. (6.73) is of the first order in the time derivative, the initial distribution $\phi(r,o)$ (over all space) must be specified. The initial time is taken when the materials in the beam region is at the initiation temperature T_R and $N_B = N_{BR}$. No diffusion has occurred yet and the distributions are

$$T(r,o) = \begin{cases} T_R & r < a \\ T_o & r > a \end{cases} \tag{6.74a}$$

$$N_B(r,o) = \begin{cases} N_{BR} & r < a \\ 0 & r > a \end{cases} \tag{6.74b}$$

Also

$$N_A(r,o) = 1 - N_B(r,o) \tag{6.74c}$$

Since Eq. (6.73) is of the second order in the spatial derivatives, two spatial boundary conditions need to be specified for each region. conservation at the boundaries requires, for both N_B and T,:

$$j_I(o,t) = 0 \qquad \text{(no source at } r = 0) \tag{6,75a}$$

$$j_I(R,t) = j_{II}(R,t) \tag{6.75b}$$

$$j_{II}(\infty,t) = 0 \qquad \text{(no source at infinity)} \tag{6.75c}$$

For the temperature at R(t), local thermal equilibrium requires

$$T_I(R,t) = T_{II}(R,t) = T_R \tag{6.76a}$$

This is essentially the defining equation for R(t), since T_R is given as the initiation temperature. Similarly for N_B,

$$N_{BI}(R,t) = N_{BII}(R,t) = N_{BR} \tag{6.76b}$$

This last equality is an assumption of constancy which is reasonable for the quasi-steady state behavior which is observed. Also

$$N_A(R,t) = 1 - N_B(R,t)$$

Eqs. (6.75) and (6.76) are appropriate sufficient conditions to produce a unique

solution for $N_A(r,t)$, $N_B(r,t)$ and $T(r,t)$.

A useful relation at the front can be obtained as follows: Perform a volume integral on Eq. (6.73) between the limits R(t) - b and R (t) + b' (b, b' fixed); apply Gauss' theorem; taking account that the limits of integration are time dependent; finally let $b \to 0$ and $b' \to \infty$ The result is:

$$\frac{d}{dt}\int_{R(t)}^{\infty} \phi_{II}(r,t)\,r\,dr + \frac{d\,R(t)}{dt}\,\phi(R,t)\,R(t) - R(t)\,j_{\phi}(R,t) = \int_{R(t)}^{\infty} S_{\phi}(r,t)\,r\,dr \qquad (6.77)$$

It will now be assumed that penetration of both heat and gas into region II is small, thus the integrals in Eq. (6.77) will be neglected. Specifically, then,

$$R\,j_{N_B}(R,t) = -\frac{D_N}{T_R}\,R\,\frac{\partial}{\partial r}(N_B T)\Big/_{r=R} = N_{BR}\,R\,\frac{dR}{dt} \qquad (6.78a)$$

$$c_v \cdot R\,j_T(R,t) = -c_v D_T R\,\frac{\partial T}{\partial r}\Big/_{r=R} = E_R\,R\,\frac{dR}{dt} \qquad (6.78b)$$

where $E_R = c_v(T_R - T_o)$ is the energy required to produce a change in temperature $T_R - T_o$. E_R is obtained from adiabatic experiments. From the basic definition of j_{N_B} as given by Eq. (6.14), it follows

$$j_{N_B}(R\,t) = N_{BR}\,V_R = N_{BR}\,\frac{dR}{dt} \qquad (6.79a)$$

and if $N_{BR} \neq 0$,

$$V_R = \frac{dR}{dt} \qquad (6.79b)$$

This completes the formal development of the model equations. It must be emphasized that the basic material "point" is actually a small macroscopic volume inside of which no microscopic modeling has been given. Caution must be exercised in interpretation. Since temperature measurement, by means of thermocouples, is the primary means of obtaining information, a discussion is appropriate.

It has been assumed that the presence of gas products is necessary to account for the observed rapid flow of heat into the cold region of the HE. Microscopic heat transfer from the gas in the porous channels to the grains of HE is likely governed by the true thermal diffusivity of the HE grains for which $D_s \sim 10^{-4}$ cm^2/sec.
In Section 3, the time scale associated with initiation propagation was estimated be $t_i \sim 15 \times 10^{-3}$ sec in PBX-9404. An associated thermal penetration distance into the solid is

$$d_l = \sqrt{D_s t_l} \sim 10^{-3}\ \text{cm} \tag{6.80}$$

Thus, the actual amount of HE material (not in the beam region) that will be brought up to $T \geq T_R$ will depend on the morphology of the material, i.e., the grain size distribution and packing density; grains with $d > d_l$ will be incompletely heated. This has bearing on μ_o, the microscopic mass density of reacting material which should not be identified with ρ_o, the true mass density of the HE material. According to Eq. (6.68a), for the quasi-steady state, μ_o will only enter results through the thermal diffusivity $D_T = \kappa/\mu_o \hat{c}_v$; there is thus no need to specify μ_o; D_T is obtained from the experimental data.

The thermocouples are in contact with the hot gases and the surface of the solid grains; the measured temperature is therefore the temperature of the porous channels through which it is assumed that the heat is being conducted.

In summary then, it has been argued, by consistent application of experimental observations in reducing the fundamental hydrodynamic-reaction equations, that transport of mass, momentum, and energy is essentially diffusive during the observed initiation propagation phase. The basic equations for the temperature T and the true gas pressure P are

$$\frac{\mu}{\mu_o}\frac{\partial T}{\partial t} - D_T \nabla^2 T = \frac{Q}{\hat{c}_v} K \qquad r < R \tag{6.81a}$$

$$-D_T R \frac{\partial T}{\partial r}\Big/_R = \frac{1}{2}\frac{E_R}{\hat{c}_v}\frac{dR^2}{dT} \qquad r = R \tag{6.81b}$$

and

$$\frac{\partial P}{\partial t} - D_P \nabla^2 P \cong \frac{\mu_o}{\sigma}\frac{R_g T}{(M_B/\alpha)} K \qquad r < R \tag{6.82a}$$

$$-D_P R \frac{\partial P}{\partial r}\Big/_R = \frac{1}{2} P_R \frac{dR^2}{dt} \qquad r = R \tag{6.82b}$$

where

$$\frac{\mu}{\mu_o} = 1 + \frac{M_B}{M_A}(N_A + N_B - 1) = 1 \tag{6.83}$$

and

$$K = K(N_A, N_B; T) = K(T) \tag{6.84}$$

The indicated approximations, when appropriate, render Eqs. (6.81) and (6.82) solvable without introducing N_A and N_B. In general, the following relations, involving N_A and N_B, need to be introduced:

$$P = \frac{\mu_o}{\sigma} \frac{R_g}{(M_B / \alpha)} N_B T \tag{6.85}$$

$$\frac{\partial N_A}{\partial t} = -K(N_A, N_B; T) \tag{6.86}$$

In the next section Eqs. (6.81) and (6.82) are solved under appropriately restricted conditions.

7. Solution of the Model Equation

In the previous section equations were developed for the determination of the temperature T, the fraction of unreacted HE N_A, and the fraction of reacted HE N_B, which was allowed to be mobile. Although the autocatalytic reaction model was used as a guide, the specific form of the reaction rate $K(N_A, N_B; T)$ was not specified. In Appendix B it is argued that the autocatalytic reaction rate is well modeled by

$$QK \cong \dot{q}_R \exp\left[\frac{T_\alpha}{T_R^2}(T - T_R)\right] \tag{7.1}$$

in the temperature range ($\Delta T \approx 40°$ C) needed to analyze thermal initiation propagation. In principle, if $K(N_A, N_B; T)$ were known, the values of $\dot{q}_R$ and T_α could be determined; in practice the values must be determined from experiment. The heat transport equation, Eq. (6.81a) (with $\mu \approx \mu_o$) then becomes

$$\frac{\partial T}{\partial t} - D_T \nabla^2 T = \frac{\dot{q}_R}{c_v} \exp[(T - T_R)/T_s] \tag{7.2}$$

where

$$T_s = \frac{T_R^2}{T_\alpha} \tag{7.2a}$$

Contributions from the beam energy deposition are negligible. Since no reaction products are measured, Eq. (7.2) is usefully appropriate. The boundary condition at the front is Eq. (6.78b):

$$-c_v D_T R \frac{\partial T}{\partial r}\Big/_{r=R} = \tfrac{1}{2} \frac{E_R dR^2}{dt} \tag{7.3}$$

It is appropriate to introduce dimensionless variables into Eq. (7.2):

$$\tau = \frac{t}{t_s} \tag{7.4a}$$

where

$$t_s = \frac{c_v T_R^2}{\dot{q}_R T_\alpha} = \frac{c_v T_s}{\dot{q}_R} \tag{7.4b}$$

t_s is the adiabatic time to explosion. Also

$$\vec{\chi} = \frac{\vec{r}}{r_s} \tag{7.5a}$$

where

$$r_s = \sqrt{D_T t_s} \tag{7.5b}$$

is a diffusion length. Additionally

$$w = \frac{T - T_R}{T_s} \tag{7.6}$$

Eq. (7.2) then takes the form

$$\frac{\partial w(\vec{\chi},\tau)}{\partial \tau} - \nabla^2 w(\vec{\chi},\tau) = e^{w(\vec{\chi},\tau)} \tag{7.7}$$

The boundary condition Eq. (7.3) becomes

$$-\chi \frac{\partial w}{\partial \chi} \Big/_{\chi=\chi} = \frac{1}{2} \frac{t_l}{t_s} \frac{d\chi^2}{d\tau} \tag{7.8a}$$

where

$$\chi(\tau) = \frac{R(t)}{r_s} \tag{7.8b}$$

and

$$t_l = \frac{E_R}{\dot{q}_R} \tag{7.8c}$$

In terms of the dimensionless variables, Eqs. (7.7) and (7.8a) have only one free parameter:

$$\frac{t_l}{t_s} = \frac{E_R}{c_v T_s} \tag{7.8d}$$

Note that this quantity doesn't depend on either $\dot{q}_R$ or D_T.

For PBX-9404, adiabatic experiments yield

$$E_R = 64 \text{ cal/gm} \qquad \text{(from 25° C)} \qquad (7.9a)$$
$$T_R = 553° \text{ K}$$

Although values for T_α and c_v are obtainable from thermal initiation propagation experiments, there is insufficient data to do so in the experiments under analysis. Nominal values [Ref. 6], correct in order of magnitude, will be used for estimation purpose. Thus

$$T_\alpha = 26.5 \times 10^3 °\text{K} \qquad (7.9b)$$
$$c_v = 0.4 \text{ cal/gm}$$

These values give

$$T_s = 11.5° \qquad (7.9c)$$
$$\frac{t_l}{t_s} = 14$$

Similar estimates of t_l/t_s for HBX-1 and TATB give values of 16 and 23, respectively.

The quasi-steady state equations are obtained by neglecting the time derivative in Eq. (7.7). This gives:

$$-\nabla^2 w = e^w \qquad (7.10a)$$

$$-\chi \frac{\partial w}{\partial \chi}\Big/_{\chi=\chi} = \tfrac{1}{2}\frac{d\chi^2}{d\theta} \qquad (7.10b)$$

in which

$$\theta = \frac{t}{t_l} = \frac{t_s}{t_l}\tau \qquad (7.10c)$$

is now the appropriate dimensionless time. Note that Eqs. (7.10a, b) have no free parameters. The quasi-steady state solutions will be adequate as long as

$$\frac{t_s}{t_l}\frac{\partial w}{\partial \theta} << e^w \qquad (7.11)$$

This condition will be verified after the solution to Eqs. (7.10a, b) is obtained.

In cylindrical coordinates (i.e., the particle beam case) Eq. (7.10a) take the form

$$-\frac{1}{\chi}\frac{d}{d\chi}\left(\chi\frac{dw}{d\chi}\right)=e^{w} \tag{7.12}$$

Radial symmetry has been assumed. The general solution to Eq. (7.12), obtained by standard techniques, is most conveniently expressed as follows:

$$\lambda(\chi)=e^{w(\chi)}=\frac{8\beta^2}{\chi^2}\frac{(\chi/\chi_m)^{2\beta}}{[(\chi/\chi_m)^{2\beta}+1]^2} \tag{7.13a}$$

The quantities β and χ_m are constants of integration which are determined by the spatial boundary conditions. The gradient of $w(\chi)$ is

$$\frac{\partial w}{\partial\chi}=\frac{2(\beta-1)}{\chi}-\frac{4\beta(\chi/\chi_m)^{2\beta}}{\chi[(\chi/\chi_m)^{2\beta}+1]^2} \tag{7.13b}$$

This must vanish at $\chi=0$; Thus $\beta=1$. In this case

$$\lambda(\chi)=\frac{\lambda_o}{\left[\frac{\lambda_o}{8}\chi^2+1\right]^2} \tag{7.14a}$$

$$\chi\frac{\partial w}{\partial\chi}=\frac{-\frac{1}{2}\lambda_o\chi^2}{\left[\frac{\lambda_o}{8}\chi^2+1\right]} \tag{7.14b}$$

where

$$\lambda_o=\lambda(\chi=0)=\frac{8}{\chi_m^2} \tag{7.14c}$$

The remaining constant of integration is obtained from the boundary condition at the front; i.e., at $\chi=X$ where $w(X)=0$, thus

$$\lambda(X)=1=\frac{\lambda_o}{\left[\frac{\lambda_o}{8}X^2+1\right]^2} \tag{7.15a}$$

Since the frontal position X is varying in time, so is λ_o; in this manner the solution

w becomes time dependent is a very specific way which is the essence of the quasi-steady state.

The solution for λ_o as a function of X can be expressed in the following convenient forms.

$$\frac{1}{\frac{\lambda_o}{8}X^2+1}=\frac{1\pm\sqrt{1-X^2/_2}}{2} \tag{7.16a}$$

or

$$\lambda_o(X)=4\left(\frac{1\mp\sqrt{1-X^2/_2}}{X^2/_2}\right)^2 \tag{7.16b}$$

The fact that λ_o must be real places a crucial restriction on $X^2/_2$, namely,

$$\frac{X^2}{2}\le 1 \tag{7.17a}$$

With the upper sign in Eq. (7.16b), the value of λ_o increases when X increases, whereas, with the lower sign λ_o decreases when X increases. clearly the upper sign corresponds to the physically observed quasi-steady state behavior; Thus

$$\lambda\le 4 \tag{7.17b}$$

Using Eqs. (7.10b) and (7.14b), the boundary condition for the flux becomes

$$\frac{1}{2}\frac{dX^2/_2}{d\theta}=\frac{\lambda_o X^2}{\left[\frac{\lambda_o}{8}X^2+1\right]} \tag{7.18a}$$

Using Eqs. (7.16a, b), this becomes

$$\frac{dX^2/_2}{d\theta}=2\left(1-\sqrt{1-X^2/_2}\right) \tag{7.18b}$$

This is the equation that governs the frontal motion as a function of time. The solution for θ is

$$\theta - \theta' = \left[\sqrt{1 - X^2/2} + \ln\left(1 - \sqrt{1 - X^2/2}\right)\right]_{X'}^{X} \tag{7.19a}$$

In terms of the original variables this becomes

$$t - t' = t_1\left[\sqrt{1 - R^2/2\,r_s^2} + \ln\left(1 - \sqrt{1 - R^2/2\,r_s^2}\right)\right]_{R'}^{R} \tag{7.19b}$$

Eq. (7.19b) gives the time for the initiation front to traverse the distance between R' and R. a comparison with experimentally observed traversal times can test the model and also produce values of r_s and t_1. This will be taken up in the next section.

The limiting value of R, from Eq. (7.18a) is

$$R^* = \sqrt{2}\, r_s \tag{7.20}$$

Since it is expected that initiation propagation will begin in the vicinity of the beam edge (i.e., the collimation radius), it follows that

$$a < R^* \tag{7.21}$$

is a necessary condition for propagation. If the beam radius is greater than R^* an explosion will develop on time scale $t_s \approx 1$ msec.

The simple model presented in Section 5 is obtained by letting D_T (and thus r_s) increase indefinitely such that

$$\frac{R^2}{2\,r_s^2} << 1 \tag{7.22}$$

Eq. (7.19b) then becomes, to first order in $1/r_s^2$,

$$t - t' \cong t_1\left[2 \ln \frac{R}{R'} - \frac{1}{4}\,\frac{R^2 - R'^2}{r_s^2}\right] \tag{7.23}$$

The first term in the expansion, with $R' = a$, $t' = t_0$, agrees with Eq. (5.6) of the simple model.

Attention will now turn to the conditions for which the quasi-steady state approximation holds. Eq. (7.11) is conveniently put into the form

$$-\frac{t_s}{t_I}\frac{\partial}{\partial\theta}\frac{1}{\lambda} << 1 \tag{7.24}$$

The time dependence of the quasi-steady state solution comes only through its dependence on the frontal variable X. From Eq. (7.14a)

$$\frac{1}{\lambda} = \frac{1}{\lambda_o}\left[\chi^2\frac{\lambda_o}{8} + 1\right]^2 \tag{7.25}$$

Eq. (7.16b) can be rearranged (with the upper sign) to give

$$\frac{1}{\lambda_o} = \frac{1}{4}\left(1 + \sqrt{1 - X^2/_2}\right)^2 \tag{7.26a}$$

These equations and Eq. (7.12b) are used to evaluate Eq. (7.24) with the results

$$\frac{t_s}{t_I}\left[1 - \left(\frac{\chi^2}{2}\right)\left(\frac{\lambda_o}{4}\right)^2\right]\frac{1}{2}\frac{X^{3/2}}{\sqrt{1 - X^{3/2}}} << 1 \tag{7.26b}$$

This must hold for any fixed point $\chi < X$. The condition is least favorable for $\chi = 0$; thus only this point needs to be considered. From Eq. (7.9c) $t_s/t_I = 1/14$ for PBX-9404; thus

$$C(X/\sqrt{2}) \equiv \frac{1}{28}\frac{X^2/_2}{\sqrt{1 - X^2/_2}} << 1 \tag{7.27}$$

A table for $C(X/\sqrt{2})$ follows:

$X/\sqrt{2}$	$C(X/\sqrt{2})$
.7	.025
.8	.038
.9	.066
.95	.103
.99	.248
.999	.797

The quasi-steady state approximation is clearly justified over essentially all of the propagation region. As the initiation front approaches close to the limiting radius R^*, the temperature rate at the origin undergoes a very rapid increase. At this point in time the dominant time scale changes rapidly from t_I to $t_s << t_I$ and an explosion develops. This warrants referring to R^* as the explosion radius. These conclusions depend on an assumed value for T_α; however, halving this value

(and thus doubling t_s/t_l) doesn't greatly alter the conclusions.

8. Model Parameters from Experiments

The model presented in the previous sections, in particular the quasi-steady state solution to the heat transport equation, allows a comparison with experiment that can produce the three scale parameters

$$t_l = \frac{E_R}{\dot{q}_R} \tag{8.1a}$$

$$r_s = \sqrt{D_T t_s} \tag{8.1 b}$$

$$T_s = \frac{T_R^2}{T_\alpha} \tag{8.1 c}$$

The time scale parameter for the non-steady state,

$$t_s = \frac{\bar{c}_v T_s}{\dot{q}_R} = t_l \frac{\bar{c}_v T_s}{E_R} \tag{8.2}$$

can then be obtained directly.

Comparison of the observed frontal motion with

$$t - t' = t_l \left[\sqrt{1 - \frac{R^2}{2 r_s^2}} + \ln \left(1 - \sqrt{1 - \frac{R^2}{2 r_s^2}} \right) \right]_R^{R^*} \tag{8.3}$$

for at least three positions (two difference) will yield values of t_l and r_s. If the explosion radius R^* is ascertained, then

$$r_s = \frac{R^*}{\sqrt{2}} \tag{8.4}$$

is determined directly. Once t_l and r_s are determined, Eqs. (8.3) gives R as an implicit function of time. According to Eqs. (7.19 a, b), λ_0 and λ are then known as a function of time and position. It then follows that

$$\frac{T(r, t) - T_R}{T_s} = w = \ln \lambda \tag{8.5}$$

can be calculated; comparison with temperature data will then yield a value for T_s.

A proper test of the model, and the extraction of accurate model parameters requires sufficient amounts of data to make any conclusion statistically significant. As was mentioned previously, the available data on thermal initiation propagation is taken from exploratory experiments performed prior to the present analysis. The most quantitative detail is obtained from one laser beam run and two particle beams runs, all on PBX-9404.

The laser case has the best temporal resolution and shows details of the frontal structure (see fig. A. 2, lower left). In particular the frontal temperature, indicated by the break in the temperature slope, agrees with the value $T_R = 280°$ C obtained in the accurate adiabatic experiments. The temperature was monitored only at one position in addition to the metal - HE interface. Time is measured from when the laser was turned on. Although this information is conceptually very valuable, it is insufficient for extracting model parameters. For this reason the solution to the model equations for planar geometry although obtained, are not presented in this report.

The particle beam data (e.g. Fig. A.1) has poor temporal resolution; however sufficient information is available to estimate t_1 and r_s. Time of arrival of the front at two spatial positions can be estimated. The time is relative to when initiation occurs at the center of the beam. The pertinent information for the two runs is abstracted is the following table:

$$a_{coll} = 0.238 \text{ (collimation radius)}$$

Position	R(cm)	t(msec)		
		I	II	Nominal
1	.476	22.2	19.4	20
2	.952	38.9	(explosion)	38*

Table 8.1

The accuracy of the time values is judged to be about 30%. In run II an explosion occurred before the thermocouple at position 2 indicated thermal initiation. Since initiation was indicated at this position in run I it is judged that the average explosion radius occurs in the vicinity of R_2, i.e.,

$$R^* = .95 \text{ cm} \tag{8.6}$$

this immediately gives

$$r_s = R^*/\sqrt{2} = .673 \text{ cm} \tag{8.7}$$

Defining

$$F(X) = \sqrt{1-\frac{X^2}{2}} + \ln\left(1-\sqrt{1-\frac{X^2}{2}}\right), \tag{8.8}$$

and using Eq. (8.3),

$$t_1 = \frac{t_2 - t_1}{F(X^*_2) - F(X_1)} \tag{8.9}$$

and since

$$F(X^*_2) = 0, \tag{8.10a}$$

$$F(X_1) = F\left(\frac{R_1}{2r_s}\right) = -1.144 \tag{8.10b}$$

$$t_2 - t_1 = 18 \text{ msec (nominal)} \tag{8.10c}$$

it follows that

$$t_1 = 15.7 \text{ msec} \tag{8.11}$$

Now that r_s and t_1 have been determined, Eq. (8.3) can be used to obtain the time difference of the arrival of the front at two positions in the propagation region.

Quasi-steady state propagation originates in the vicinity of the beam edge at a position which will be denoted by a_{eff}; furthermore quasi-steady state propagation is established, presumably, on a time scale $t_s \approx 1$ msec after initiation has begun. It follows that the absolute times in table 8.1 are essentially the time differences from a_{eff} to the indicated position. These considerations allow a determination of a_{eff}. Using the information at position 2 for which $F(X_2) = 0$, Eq. (8.3) gives

$$F\left(\frac{a^2_{eff}}{2r_s^2}\right) = -\left(\frac{t_2}{t_1}\right) = -2.42$$

Thus

$$\frac{a^2_{eff}}{2r_s^2} = .133$$

$$a_{eff} = .245 \text{ cm}$$

The information at position 1, of necessity, gives the same result. In view of the uncertainties in the data, the small (4%) difference in a_{eff} and a_{coil} is perhaps

fortuitous; however it does indicate consistency in the model application.

The value of T_s cannot be obtained from the particle beam data since the latter does not give the temporal development of the temperature above T_R. The laser beam data gives this information, but the frontal motion is not known with much certainty. For further application the values of T_s or t_s/t_l given by Eq. (7.9c) will be used. An uncertainty by a factor of two is judged to be conservative.

Values of $\dot{q}_R$ and D_T can now be estimate as follows:

$$\dot{q}_R = \frac{E_R}{t_l} = 4 \times 10^3 \text{ cal/gm-sec} \tag{8.12}$$

$$D_T = \frac{r_s^2}{t_s} = \frac{r_s^2}{t_l}\frac{t_l}{t_s} = 0.4 \times 10^3 \text{ cm}^2/\text{sec} \tag{8.13}$$

The magnitude of $\dot{q}_R$ justifies neglect of the beam term ($\dot{q}_b \approx 10$ cal/gm-sec); it also indicates that radical change in the reaction has occurred at T_R, the initiation temperature. The large magnitude of the thermal diffusivity D_T indicated that normal condensed matter thermal conductivity is not taking place (For Aluminum $D_T \approx 1$ cm^2/sec). It's explanation is beyond the macroscopic analysis present in this study.

9. Conclusions

Many features of the thermal initiation propagation experiments described in Appendix A.1 and Reference 2 can be accounted for through the diffusion-reaction equation (7.2) with the dynamical boundary conditions given by Eq. (7.3) . The quasi-steady state assumption gives rise to the equation (7.20):

$$t - t' = t_1\left[\sqrt{1-(R/R^*)^2} + \ln\left(1-\sqrt{1-(R/R^*)^2}\right)\right]_R^R \tag{9.1}$$

which describes the propagation of the thermal initiation front quite adequately until the position R^* is reached.

Detailed quantitative validation of the front propagation equation has not been given owing to the sparseness of useful data. There is sufficient qualitative and order of magnitude experimental information to allow a reduction of the general hydrodynamical-reaction equations to the basic equations (7.2) and (7.3).

The existing quantitative data for PBX-9404 allows for an approximate determination of t_1 and R^*; these in turn yield a value for the exothermic rate and, with an order of magnitude assumption for the effective activation temperature, the effective diffusivity, D_T. If reliable temperature readings behind the front were available, a value of the effective activation temperature, T_α, could be obtained directly.

The values

$$\dot{q}_R = 4 \times 10^3 \text{ cal/gm-sec}$$

$$D_T = 0.4 \times 10^3 \text{ cm}^2/\text{sec} \tag{9.2}$$

do not resemble the values inferred from Ref. (6) which are

$$\dot{q}_R = 39 \text{ cal/gm-sec}$$

$$D_T = 9.7 \times 10^{-4} \text{ cm}^2/\text{sec} \tag{9.3}$$

The values are obtained as follows (with $T_R = 553°K$)

$$\dot{q}_R = Z Q \exp(-T_\alpha/T_R)$$

$$D_T = \kappa/\rho c_v$$

where

$$Z = 5 \times 10^{19}\ \text{sec}^{-1},\ Q = 500\ \text{cal/gm},\ T_\alpha = 26.5 \times 10^3\text{°K}$$
$$\rho = 1.81\ \text{gm/cm}^3,\ c_v = 0.4\ \text{cal/gm-deg}$$
$$\kappa = 7 \times 10^{-4}\ \text{cal/cm-sec-deg}$$

These data were obtained from experiments (DSC, etc) performed below the initiation temperature T_R. A 10% reduction in T_α would bring the values of $\dot{q}_R$ in (9.3) into agreement with the values in (9.2). The large value of D_T in (9.2) indicates a wholly different mechanism for heat transport above T_R.

The principal applications of thermal initiation theory lie in the areas of Directed Energy weapons (particle beams and high energy lasers) and in high explosives hazard analysis. The propagation phenomena reported on and analyzed in this paper are important when the dimensions of the region which first experiences thermal initiation is less than the explosion radius R^*. The theory derived here applies once propagation starts. Not enough information is available to determined all the conditions that must be met before propagation begins. A minimum size region having reached the thermal initiation temperature seems to be necessary.

Further experiments, guided by the present analysis and the work described in Appendix A.1 and Ref.(2), would greatly enhance the understanding of thermal initiation propagation.

Appendix A.1. Early NRL Propagation Experiment

In 1980, a series of experiments were performed at NRL Linac in which confined disks of HE, 1 inch diameter x 1/4 inch thick (about 6 gm), were exposed to non-uniform irradiation by a 32 - MeV electron beam with the following pulse parameters: 0.3 Amp, 1 μsec, and 360 pulses/sec. this produced a heating rate of about 9 cal/gm-sec, and resulted in thermally-induced explosions in 6 to 15 sec. The HE samples were placed in Al confinement cells, sealed with O-rings. The beam entrance window was 3/32 inch thick, and the exit window was only 1/32 inch thick, so that blast fragments should move away from the accelerator. The beam was collimated to a diameter of 3/16 inch, so it irradiates and heats only the central region of the HE. Three iron-constantan thermocouples (0.001-inch diameter) are imbedded in the rear face of the HE: one at the center (in the beam area), and two outside the beam area, at radial distances of 3/16 inch and 3/8 inch from the center. The thermocouple response time is about 2 msec. Two tests were performed on each of the following materials: TATB, HBX-1(contains TNT, RDX and Al), and PBX-9404 (Contains 94% HMX). Beam irradiation was continuous until explosion occurred.

In the TATB samples, explosions were quite weak, with no reaction spreading beyond the beam area The HBX-1 samples exploded with more violence, consuming a large portion of HE beyond the beam area. The thermocouple data indicate a slow reaction propagation velocity, of the order of 1 cm/sec. The PBX-9404 samples exploded very violently, ripping up the 3/4 inch thick aluminum back plate of the confinement cell into chunks of twisted metal. All of the HE was consumed rapidly. Temperature vs. time data (from the first run) from the three thermocouples near initiation are shown in Fig. A-1. Since the thermocouples were only a millimeter from the highly conducting rear face of the holder, they do not indicate the true temperature of the interior of the HE. They do indicate correctly the time of arrival of an initiation front indicated by an extremely rapid temperature rise. Analysis of the two PBX-9404 runs yield the following data:

$$a_{coll} = 0.238 \text{ (collimation radius)}$$

Position	R(cm)	t(msec)		
		I	II	Nominal
1	.476	22.2	194	20
2	.952	38.9	(explosion)	38*

Table A.1

The accuracy of the time values is judged to be about 30%. In run II an explosion occurred before the thermocouple at position 2 (the edge) indicated thermal initiation. Since initiation was indicated at this position in run I, it is assumed that the explosion radius (as defined in the main text) occurs in the neighborhood of position 2. The data indicated a propagation speed of about 25-35 cm/sec.

Recent data (1990, Ref (2)), also obtained at the NRL Linac, do not indicate a time difference between initiation at the center and the outer regions. However, these data were obtained under rather different conditions: a wider beam (1/2 inch diameter), a slower beam heating rate (3 cal/gm-sec), and using thermocouples with a longer response time (40 msecs). These experiments were performed without the benefits of the analysis presented in this paper. More pertinent results would require a narrower beam (≤ 1/8 inch diameter), a shorter time response in the thermocouple (≤ 2 msec). Better time resolution in time recording is also indicated. Finally, the thermocouple should be buried deeper (about half way) into the interior of the HE so that a true profile of the propagation temperature can be obtained.

In November, 1983, thermal initiation experiments were performed with the Repetively Pulsed Chemical Laser (RPCL) at the TRW facility in Capistrano, CA. The experimental arrangement was as follows:

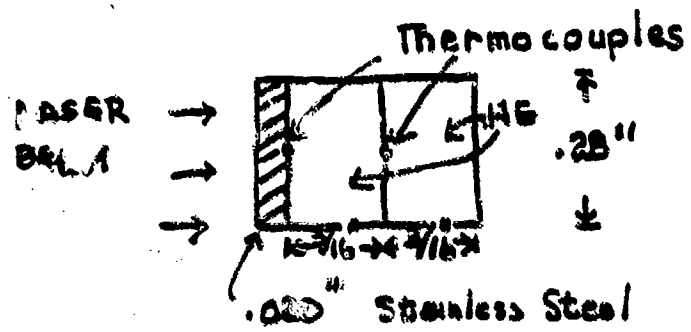

The laser beam heats the outer face of the steel plate. Thermal conduction through the steel plate then produces a temperature rise at the interface between the plate and the HE. One thermocouple (the same type as used in the Linac experiments) was placed at the interface, the other was placed in the middle of the HE.

The temperature-time response is depicted in Fig. A.2. the interface temperature initially rises at ~1500°c/sec till the HE melts in the vicinity of 280°C. A slowly accelerating temperature rise then occurs up to 560°C, at which point a very sharp temperature rise, indicative of intense exothermic activity, appears.

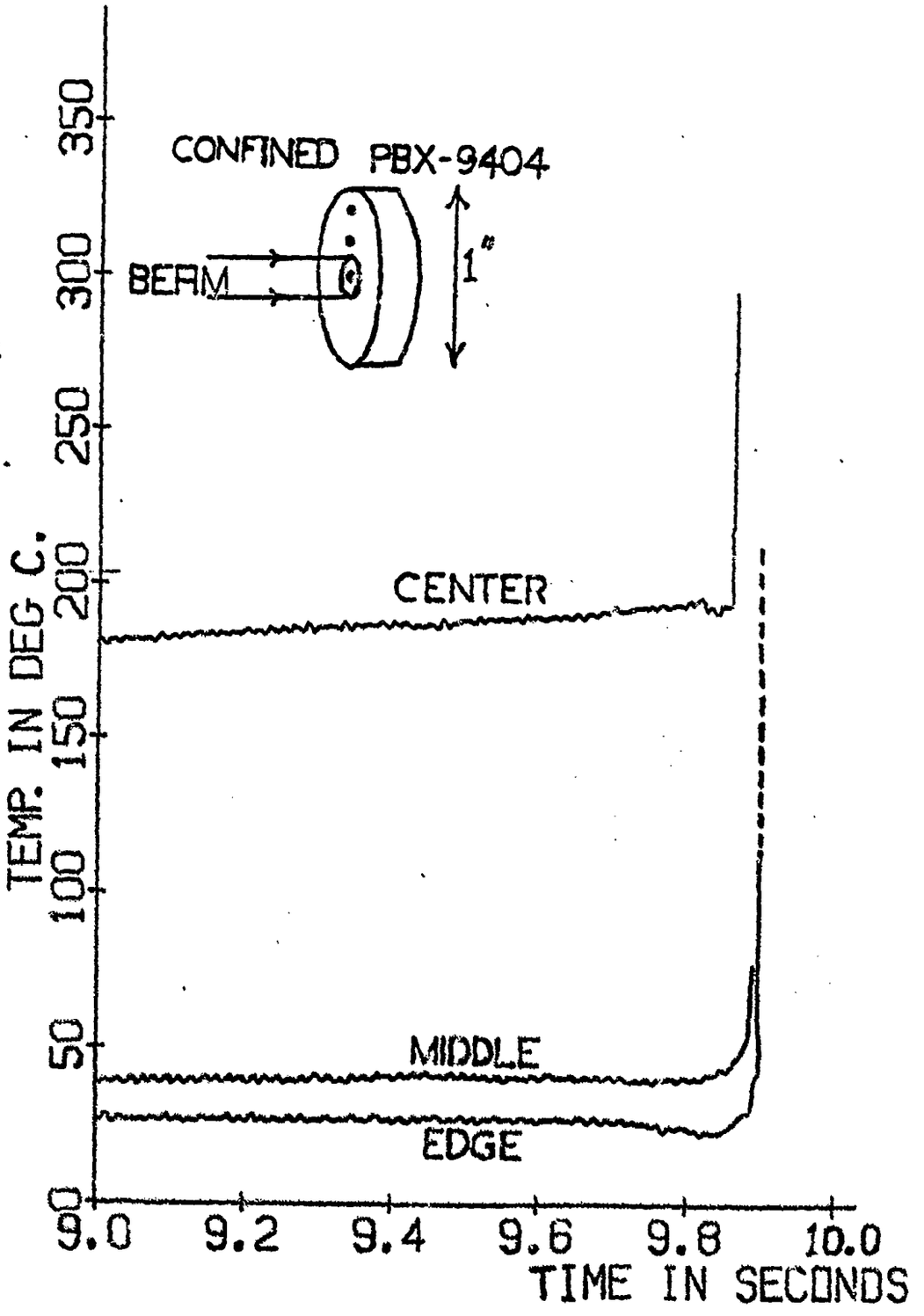
CONFINED PBX-9404
BEAM
1"
TEMP. IN DEG C.
350
300
250
200
150
100
50
0
CENTER
MIDDLE
EDGE
9.0
9.2
9.4
9.6
9.8
10.0
TIME IN SECONDS

Figure A-1

The temperature in the middle of the HE (lower left in Fig. A-2) remains unchanged (~21°C) until after the above noted exothermic appears. It then undergoes a very rapid (< 10 msec) rise to the vicinity of the thermal initiation threshold (280° ± 5°C). At this point the temperature rate is considerably reduced. The precise structure of the temperature profile would require accounting for the finite (~2 msec) response time of the thermocouple. However, the profile is consistent with the propagating front structure described in the main text.

Quantitative analysis of the frontal motion cannot be made since it is not known when and where a steady state initiation front began. This would required information from one or more additional measurements in the interior of the HE. Various assumptions result in an estimated frontal speed of 20-90 cm/sec. The order of magnitude is consistent with the particle beam result.

The laser experiment gives information on what occurs when only one surface of HE is rapidly heated. The observation that the interface region of the HE reaches a temperature considerably above the thermal initiation threshold ($T_R = 280° \pm 5°$) shows that temperature alone does not determine the precipitation of initiation propagation. It is probable that a certain threshold volume has to be brought up to T_R or beyond before propagation commences. In the particle beam experiments, which produced rapid volumetric heating, the threshold volume was apparently exceeded. Quantitative information in this matter is needed to complete the understanding of the propagation phenomenon.

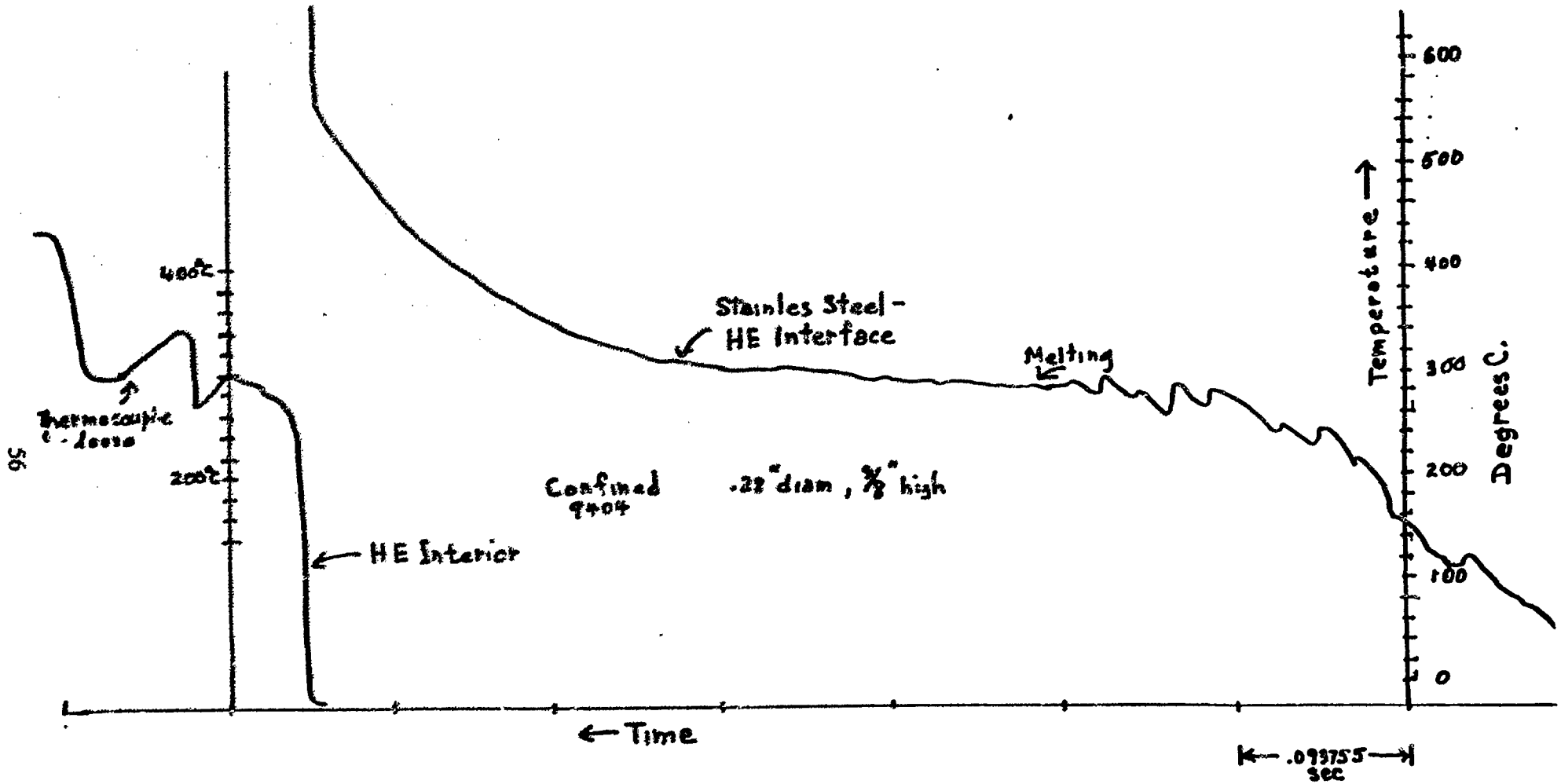
400°C
200°C
Thermocouple Leads
Stainless Steel - HE Interface
Melting
Confined 9404
.22" diam, 3/8" high
HE Interior
Time
.093755 sec
Temperature
Degrees C.
600
500
400
300
200
100
0

Figure A-2

Appendix A.2. Reaction Model Equivalencies

It will be assumed that the exothermic heating rate can be represented as a function only of the temperature:

$$Q K = \dot{q}_R G(T) \qquad (A.2 - 1)$$

in which $\dot{q}_R$ is the exothermic heating rate at the temperature T_R. In general, since $G(T_R) = 1$,

$$\ln G(T) = a_1 (T-T_R) + 1/2\, a_2 (T-T_R)^2 + \ldots \qquad (A.2 - 2)$$

where

$$a_1 = \frac{d \ln G}{dT}\Big/_R, \quad a_2 = \frac{d^2 \ln G}{dT^2}\Big/_R, \text{etc.} \qquad (A.2 - 3)$$

In the simplest case

$$K^{(A)} = Z_A e^{-\frac{T_A}{T}} \qquad (A.2 - 4)$$

for which

$$T_R^2 \frac{d G^{(A)}}{dT}\Big/_R = T_A \qquad (A.2 - 5)$$

Thus, in general, when the first term in (A.2 - 2) is an adequate approximation,

$$T_R^2 \frac{d G}{dT}\Big/_R \equiv T_\alpha \qquad (A.2 - 6)$$

can be construed as an effective activation temperature.

A necessary condition for the adequacy of the approximation is

$$1/2 |a_2| (T - T_R)^2 << 1 \qquad (A.2 - 7)$$

Consideration of the autocatalytic reaction rate

$$K = N_A (Z_A e^{-\frac{T_A}{T}} + Z_B N_B e^{-\frac{T_B}{T}}) \qquad (A.2 - 8)$$

requires knowledge of the temperature dependence of N_A and N_B. In adiabatic uniform self-heating,

$$\frac{dN_A}{dt} = -K, \quad \frac{dN_B}{dt} = K$$
$$c_v \frac{dT}{dt} = QK \qquad \text{(A. 2 - 9)}$$

The first two equations are equivalent to

$$-\frac{dN_A}{dT} = \frac{dN_B}{dT} = \frac{c_v}{Q} \qquad \text{(A. 2 - 10)}$$

which have the solution

$$\frac{N_A}{N_{AR}} = \left(1 - \frac{N_{BR}}{N_{AR}} \frac{c_v(T - T_R)}{E_R}\right)$$
$$\frac{N_B}{N_{BR}} = \left(1 + \frac{c_v(T - T_R)}{E_R}\right) \qquad \text{(A.2 - 11)}$$

where $E_R = N_{BR}Q$ has been used. For PBX-9404, $c_v \approx .4$ cal/gm-deg, $E_R \approx 64$ cal/gm, then for $N_{BR}/N_{AR} \approx 1/10$ and $T - T_R \approx 40°$ C,

$$\frac{c_v(T - T_R)}{E_R} \approx .25, \quad \frac{N_{BR}}{N_{AR}} \frac{c_v(T - T_R)}{E_R} \approx .025$$

Exponentiation is achieved with the relation

$$1 + x \equiv e^{\ln(1+x)} \equiv e^{x - \frac{x^2}{2} + \cdots} \qquad \text{(A.2 - 12)}$$

For N_A/N_{AR} the first term in the exponent is an adequate approximation for $T - T_R \leq 40°C$; its only effect is to make a contribution to T_α in the amount

$$T_R^2 \frac{d \ln \frac{N_A}{N_{AR}}}{dT}\Big/_R = -T_R^2 \frac{c_v}{Q} \approx -.19 \times 10^3 \, °K \qquad \text{(A.2 - 13)}$$

with $T_R \approx 553°K$. Since $T_\alpha \approx 26.5 \times 10^3 °K$, the contribution from N_A is quite small. Henceforth the variation in N_A will be neglected in both adiabatic self heating and in the QSS propagation process.

In QSS propagation the defining equations for N_B and T are

$$-D_N \nabla^2 (N_B\ T) = K$$
$$-D_T \nabla^2 T = \frac{Q}{c_v} K \qquad \text{(A.2 - 14)}$$

which give

$$D_N N_B T - D_T \frac{c_v}{Q} T = \text{const}$$

or (A.2- 15)

$$\frac{N_B}{N_{BR}} = \frac{1 + \frac{D_T}{D_N} \frac{c_v}{E_R} (T - T_R)}{1 + \frac{1}{T_R} (T - T_R)}$$

Although no knowledge of D_N is at hand, the assumption that thermal diffusion is intimately dependent on gaseous diffusion leads to the conclusion that D_N and D_T have the same order of magnitude. Thus the variation of N_B with temperature does not differ significantly in magnitude between adiabatic self heating and QSS propagation. It is adequate to assume

$$\frac{N_B}{N_{BR}} \cong e^{\xi (T - T_R) - \frac{\xi^2}{2} (T - T_R)^2} \qquad \text{(A.2 - 16)}$$

where, for purpose of estimation, $\xi \approx \frac{c_v}{E_R} \approx .0063$.

The function G(T) is conveniently put into the form

$$G(T) = k \exp\left(\frac{T_A}{T_R} - \frac{T_A}{T}\right) + (1 - k) \exp\left(\frac{T_B}{T_R} - \frac{T_B}{T} + \ln \frac{N_B}{N_{BR}}\right) \qquad \text{(A.2 - 17)}$$

where

$$k = Z_A \exp\left(-\frac{T_A}{T_R}\right)\left(Z_A \exp - \frac{T_A}{T_R} + Z_B N_{BR} \exp - \frac{T_B}{T_R}\right)^{-1} \qquad \text{(A.2 -18)}$$

(and N_A/N_{AR} is set to unity). The ratio of the first to second term of G(T) at T = T_P is given by

$$x_R = \frac{1 - k}{k}$$

thus (A.2-19)

$$k = \frac{1}{1 + x_R}$$

and

$$0 \le x \le \infty, \qquad 1 \ge k \ge 0 \tag{A.2 - 20}$$

On applying Eq. (A.2 - 3), the following basic relations are obtained:

$$T_\alpha = k\,T_A + (1-k)(T_B + \xi\,T_R^2) \tag{A.2 - 21}$$

$$g_2 = \frac{1}{2}\,a_2 (T - T_R)^2 = \left\{ -\frac{T_R}{T_a}\left[1 - (1-k)\,\xi\,T_s\left(1 - \frac{\xi\,T_R}{2}\right)\right] + \frac{k(1-k)}{2}\left[\frac{T_B - T_A}{T_\alpha} + \xi\,T_s\right]^2 \right\} \left(\frac{T - T_R}{T_s}\right)^2 \tag{A.2 - 22}$$

where $T_s = T_R^2/T_\alpha$. For PBX-9404, $T_R = 553°K$, $T_\alpha \approx 26.5 \times 10^3 °K$; using $\xi = .0063$ it follows that $T_s = 11.54°$, $\xi T_s = .073$, $\xi T_R/2 = 1.74$. The ξ dependent part of the first term in (A.2 - 22) is seen to be negligible. Thus

$$\frac{1}{2}\,a_2 (T - T_R)^2 = \left\{ -.021 + \frac{k(1-k)}{2}\left[\frac{T_B - T_A}{T_\alpha} + 0.73\right]^2 \right\} \left(\frac{T - T_R}{T_s}\right)^2 \tag{A.2 - 23}$$

Without specific knowledge of x_R and $T_B - T_A$ it is necessary to consider extremal cases. At the extremes $k = 0, 1$ ($x_R = \infty, 0$),

$$\text{EXTREME} \quad g_2 = -.021 \left(\frac{T - T_R}{T_s}\right)^2 \tag{A.2 - 24}$$

The coefficient a_2 is maximized at $k = 1/2$ ($x_R = 1$)

$$\text{MAXIMUM} \quad g_2 = \left\{ -.021 + \frac{1}{8}\left(\frac{T_B - T_A}{T_\alpha} + 0.73\right)^2 \right\} \left(\frac{T - T_R}{T_s}\right)^2 \tag{A.2 - 25}$$

The maximum exceeds the magnitude of the extreme value only when

$$\frac{T_B - T_A}{T_\alpha} < -.635 \quad (T_B < T_A)$$

or (A.2 - 26)

$$\frac{T_B - T_A}{T_\alpha} > .507 \quad (T_B > T_A)$$

Thus for a considerable range of values of $T_B - T_A$ and for all values of k (or x_R),

$$\frac{1}{2}|a_2|\left(\frac{T-T_R}{T_s}\right)^2 < .021\left(\frac{T-T_R}{T_s}\right)^2 << 1 \qquad \text{(A.2 - 27)}$$

can be taken as a rather conservative condition for the validity of the first approximation.

In QSS propagation the maximum value of $(T - T_R)/T_s$ is $\ln 4 = 1.386$ ($\Delta T \equiv$ 16°C), thus

$$\frac{1}{2}|a_2|\left(\frac{T-T_R}{T_s}\right)^2 < .04$$

More generally, when $T - T_R \leq 40°C$,

$$\frac{1}{2}|a_2|\left(\frac{T-T_R}{T_s}\right)^2 < .25$$

This is probably the limit for which the approximation is useful.

In summary, the analysis shows (1) that the simple form

$$Q\,K = \dot{q}_R\, e^{\frac{T_s}{T_R^2}(T-T_R)}$$

can be deduced from more complex forms and used for a limited temperature range and (2) the analysis of data for a limited temperature range $\Delta T \leq 40°C$ can only yield two reaction parameters, $\dot{q}_R$ and T_ω; more complex modeling is inappropriate.

REFERENCES

1. "Thermal Initiation of High Explosives by Electron Beam Heating", A. Stolovy, A. I. Namenson, J. B. Aviles, Jr., E. C. Jones, Jr., and J. M. Kidd. J. of Energetic Materials, 5, 181-238 (1987).

2. "Reaction Propagation Studies in Beam-Initiated Confined Explosives", A. Stolovy, J. M. Kidd and A. I. Namenson, NRL Memorandum Report 6717, Oct. 8, 1990.

3. "Numerical Modeling of Detonations", C. L. Mader, Univ. of Calif. Press, 1979. See page 266, et seq.

4. "Thermochemistry of Explosives", R. N. Rogers, Thermochim. Acta 11, 131-139 (1975).

5. "Fluid Mechanics", L. D. Landau and E. M. Lifshitz, Addison-Wesley, 1959. See page 183, et seq.

6. "LLNL Explosives Handbook", B. M. Dobratz, UCRL-52997, March 16, 1981.

ACKNOWLEDGEMENT

One of us (JBA) would like to gratefully acknowledge support by Dr. David Nagel and the Civil Service Retirement System.